

*Article*

# A Responsible Machine Learning Workflow

With Focus on Interpretable Models, Post-hoc Explanation, and Discrimination Testing

Navdeep Gill <sup>1,†</sup>, Patrick Hall <sup>1,3,t,\*</sup>, Kim Montgomery <sup>1,†</sup>, and Nicholas Schmidt <sup>2,†</sup>

<sup>1</sup> H2O.ai

<sup>2</sup> BLDS, LLC

<sup>3</sup> The George Washington University

\* Correspondence: phall@h2o.ai; nschmidt@bldslc.com

† All authors contributed equally to this work.

Version February 7, 2020 submitted to Information

**Abstract:** This manuscript outlines a viable approach for training and evaluating machine learning (ML) systems for high-stakes, human-centered, or regulated applications using common Python programming tools. The accuracy and intrinsic interpretability of two types of constrained models, monotonic gradient boosting machines (MGBMs) and explainable neural networks (XNNs), a deep learning architecture well-suited for structured data, are assessed on simulated data and publicly available mortgage data. For maximum transparency and the potential generation of personalized adverse action notices, the constrained models are analyzed using post-hoc explanation techniques including plots of partial dependence (PD) and individual conditional expectation (ICE) and with global and local Shapley feature importance. The constrained model predictions are also tested for disparate impact (DI) and other types of discrimination using measures with long-standing legal precedents, adverse impact ratio (AIR), marginal effect (ME), and standardized mean difference (SMD), and also with straightforward group fairness measures. By combining interpretable models, post-hoc explanations, and discrimination testing with accessible software tools, this text aims to provide a template workflow for important ML applications that require high accuracy and interpretability and that mitigate risks of discrimination.

**Keywords:** Deep Learning; Disparate Impact; Explanation; Fairness; Gradient Boosting Machine; Interpretable; Machine Learning; Neural Network; Python

## 0. Introduction

Responsible artificial intelligence (AI) has been variously conceptualized as AI-based products or projects that use transparent technical mechanisms, that create appealable decisions or outcomes, that perform reliably and in a trustworthy manner over time, that exhibit minimal social discrimination, and that are designed by humans with diverse experiences, both in terms of demographics and professional backgrounds.<sup>1</sup> Although responsible AI is today a somewhat broad and amorphous notion, at least one aspect is becoming clear. ML models, a common application of AI, can present serious risks. ML models can be inaccurate and unappealable black-boxes, even with the application of newer post-hoc explanation techniques [1].<sup>2</sup> ML models can perpetuate and exacerbate discrimination [2], [3], [4], and ML models can be hacked, resulting in manipulated model outcomes or the exposure

<sup>1</sup> See: [Responsible Artificial Intelligence, Responsible AI: A Framework for Building Trust in Your AI Solutions](#), PwC's Responsible AI, Responsible AI Practices.

<sup>2</sup> See: [When a Computer Program Keeps You in Jail](#).

of proprietary intellectual property or sensitive training data [5], [6], [7], [8]. This manuscript makes no claim that these interdependent issues of ML opaqueness, discrimination, privacy harms, and security vulnerabilities have been resolved, even as singular entities, and much less as complex intersectional phenomena. However, Sections 1, 2, and 3 do propose some specific technical countermeasures, mostly in the form interpretable models, post-hoc explanation, and DI and discrimination testing, that responsible practitioners can use to address a subset of these vexing problems.<sup>3,4</sup>

Section 1 describes methods and materials, including training datasets, interpretable and constrained models, post-hoc explanations, tests for DI and other social discrimination, and public and open source software resources associated with this text. In Section 2, interpretable and constrained modeling results are compared to less interpretable and unconstrained models, and post-hoc explanation and discrimination testing results are also presented for interpretable models. Of course, an even wider array of tools and techniques are likely helpful to fully minimize discrimination, inaccuracy, privacy, and security risks associated with ML models. Section 3 puts forward a more holistic responsible ML modeling workflow, and addresses the burgeoning Python ecosystem for responsible AI, along with appeal and override of automated decisions, and discrimination testing and remediation in practice. Section 4 closes this manuscript with a brief summary of the outlined methods, materials, results, and discussion.

## 1. Materials and Methods

The simulated data (see Subsection 1.1) is based on the well-known Friedman datasets. Its known feature importance and augmented discrimination characteristics are used to gauge the validity of interpretable modeling, post-hoc explanation, and discrimination testing techniques [10], [11]. The mortgage data (see Subsection 1.2) is sourced from the Home Mortgage Disclosure Act (HMDA) database and is a fairly realistic data source for demonstrating the template workflow.<sup>5</sup> To provide a sense of fit differences, performance of more interpretable constrained ML models and less interpretable unconstrained ML models is compared on simulated data and collected mortgage data. Because the unconstrained ML models, gradient boosting machines (GBMs, e.g. [12], [13]) and artificial neural networks (ANNs, e.g. [14], [15], [16], [17]), do not exhibit convincing accuracy benefits on the simulated or mortgage data and can also present the unmitigated risks discussed above, further explanation and discrimination analyses are applied only to the constrained, interpretable ML models [1], [18], [19]. Here, MGBMs<sup>6</sup> (See Subsection 1.3) and XNNs (see Subsection 1.4, [20] [21]) will serve as those more interpretable models for subsequent explanatory and discrimination analyses. MGBM and XNN interpretable model architectures are selected for the example workflow because they are straightforward variants of popular unconstrained ML models. If practitioners are working with GBM and ANN models, it should be relatively uncomplicated to also evaluate the constrained versions of these models.

The same can be said of the selected explanation methods and discrimination tests. Due to their post-hoc nature, they can often be shoe-horned into existing ML workflows and pipelines. Presented explanation techniques include PD and ICE (see Subsection 1.5) and Shapley values (see Subsection 1.6) [13], [22], [23], [24]. PD, ICE, and Shapley values provide direct, global, and local summaries and descriptions of constrained models without resorting to the use of intermediary and approximate

<sup>3</sup> This text and associated software are not, and should not be construed as, legal advice or requirements for regulatory compliance.

<sup>4</sup> In the United States (US), interpretable models, explanations, DI testing, and the model documentation they enable may be required under the Civil Rights Acts of 1964 and 1991, the Americans with Disabilities Act, the Genetic Information Nondiscrimination Act, the Health Insurance Portability and Accountability Act, the Equal Credit Opportunity Act (ECOA), the Fair Credit Reporting Act (FCRA), the Fair Housing Act, Federal Reserve Supervisory and Regulatory (SR) Letter 11-7, and the European Union (EU) General Data Protection Regulation (GDPR) Article 22 [9].

<sup>5</sup> See: [Mortgage data \(HMDA\)](#).

<sup>6</sup> As implemented in [XGBoost](#) or [h2o](#).

68 surrogate models. Discussed discrimination testing methods (see Subsection 1.7) include AIR, ME, and  
 69 SMD [2], [25], [26].<sup>7</sup> Accuracy and other confusion matrix measures are also reported by demographic  
 70 segment [27]. All outlined materials and methods are implemented in open source Python code, and  
 71 are made available on GitHub (see Subsection 1.8).

### 72 1.1. Simulated Data

73 Simulated data is created based on a signal-generating function,  $f$ , applied to input data,  $\mathbf{X}$ , first  
 74 proposed in Friedman [10] and extended in Friedman *et al.* [11]:

$$f(\mathbf{X}) = 10 \sin(\pi X_{\text{Friedman},1} X_{\text{Friedman},2}) + 20(X_{\text{Friedman},3} - 0.5)^2 + 10 X_{\text{Friedman},4} + 5 X_{\text{Friedman},5} \quad (1)$$

75 where each  $X_{\text{Friedman},j}$  is a random uniform feature in  $[0, 1]$ . In Friedman's texts, a Gaussian noise  
 76 term was added to create a continuous output feature for testing spline regression methodologies.  
 77 In this manuscript, the signal-generating function and input features are modified in several ways.  
 78 Two binary features, a categorical feature with five discrete levels, and a bias term are introduced  
 79 into  $f$  to add a degree of complexity that may more closely mimic real-world settings. For binary  
 80 classification analysis, the Gaussian noise term is replaced with noise drawn from a logistic distribution  
 81 and coefficients are re-scaled to be  $\frac{1}{5}$  of the size of those used by Friedman, and any  $f(\mathbf{X})$  value above  
 82 0 is classified as a positive outcome, while  $f(\mathbf{X})$  values less than or equal to zero are designated as  
 83 negative outcomes. Finally,  $f$  is augmented with two hypothetical protected class-control features with  
 84 known dependencies on the binary outcome to allow for discrimination testing. The simulated data is  
 85 generated to have eight input features, twelve after numeric encoding of categorical features, and a  
 86 binary outcome, two class-control features, and 100,000 instances. The simulated data is then split into  
 87 a training and test set, with 80,000 and 20,000 instances, respectively. Within the training set, a 5-fold  
 88 cross-validation indicator is used for training all models. For an exact specification of the simulated  
 89 data, see the software resources referenced in Subsection 1.8.

### 90 1.2. Mortgage Data

91 The mortgage dataset analyzed here is a random sample of consumer-anonymized loans from the  
 92 HDMA database. These loans are a subset of all originated mortgage loans in the 2018 HMDA data that  
 93 were chosen to represent a relatively comparable group of consumer mortgages. A selection of features  
 94 is used to predict whether a loan is *high-priced*, i.e., the annual percentage rate (APR) charged was 150  
 95 basis points (1.5%) or more above a survey-based estimate of other similar loans offered around the  
 96 time of the given loan. After data cleaning and preprocessing to encode categorical features and create  
 97 missing markers, the mortgage data contains ten input features and the binary outcome, *high-priced*.  
 98 The data is split into a training set with 160,338 loans and a marker for 5-fold cross-validation and  
 99 a test set containing 39,662 loans. While lenders would almost certainly use more information than  
 100 the selected features to determine whether to offer and originate a high-priced loan, the selected  
 101 input features (loan to value (LTV) ratio, debt to income (DTI) ratio, property value, loan amount,  
 102 introductory interest rate, customer income, etc.) are likely to be some of the most influential factors  
 103 that a lender would consider. See the resources put forward in Section 1.8 and Appendix A for more  
 104 information regarding the HMDA mortgage data.

### 105 1.3. Monotonic Gradient Boosting Machines

106 MGBMs constrain typical GBM training to consider only tree splits that obey user-defined positive  
 107 and negative monotonicity constraints, with respect to each input feature,  $X_j$ , and a target feature,  $y$ ,

---

<sup>7</sup> See: Part 1607 - Uniform Guidelines on Employee Selection Procedures (1978) §1607.4.

<sup>108</sup> independently. An MGBM remains an additive combination of  $B$  trees trained by gradient boosting,  
<sup>109</sup>  $T_b$ , and each tree learns a set of splitting rules that respect monotonicity constraints,  $\Theta_b^{\text{mono}}$ . For some  
<sup>110</sup> instance,  $\mathbf{x}$ , a trained MGBM model,  $g^{\text{MGBM}}$ , takes the form:

$$g^{\text{MGBM}}(\mathbf{x}) = \sum_{b=0}^{B-1} T_b(\mathbf{x}; \Theta_b^{\text{mono}}) \quad (2)$$

<sup>111</sup> As in unconstrained GBM,  $\Theta_b^{\text{mono}}$  is selected in a greedy, additive fashion by minimizing a regularized  
<sup>112</sup> loss function that considers known target labels, the predictions of all subsequently trained trees in  
<sup>113</sup>  $g^{\text{MGBM}}$ , and the  $b$ -th tree splits applied to  $\mathbf{x}$ ,  $T_b(\mathbf{x}; \Theta_b^{\text{mono}})$ , in a numeric loss function (e.g., squared loss,  
<sup>114</sup> Huber loss), and a regularization term that penalizes complexity in the current tree. See Appendices  
<sup>115</sup> [B.1](#) and [B.2](#) for details pertaining to MGBM training.

<sup>116</sup> Herein, two  $g^{\text{MGBM}}$  models are trained. One on the simulated data and one on the mortgage  
<sup>117</sup> data. In both cases, positive and negative monotonic constraints for each  $X_j$  are selected using  
<sup>118</sup> domain knowledge, random grid search is used to determine other hyperparameters, and 5-fold  
<sup>119</sup> cross-validation and test partitions are used for model assessment. For exact parameterization of the  
<sup>120</sup> two  $g^{\text{MGBM}}$  models, see the software resources referenced in Subsection [1.8](#).

#### <sup>121</sup> 1.4. Explainable Neural Networks

<sup>122</sup> XNNs are an alternative formulation of additive index models in which the ridge functions are  
<sup>123</sup> neural networks [20]. XNNs also bear a strong resemblance to generalized additive models (GAMs)  
<sup>124</sup> and so-called explainable boosting machines (EBMs or GA<sup>2</sup>M), i.e., GAMs which consider main effects  
<sup>125</sup> and a small number of 2-way interactions and may also incorporate boosting into their training [13],  
<sup>126</sup> [28]. XNNs enable users to tailor interpretable neural network architectures to a given prediction  
<sup>127</sup> problem and to visualize model behavior by plotting ridge functions. A trained XNN function,  $g^{\text{XNN}}$ ,  
<sup>128</sup> applied to some instance,  $\mathbf{x}$ , is defined as:

$$g^{\text{XNN}}(\mathbf{x}) = \mu_0 + \sum_{k=0}^{K-1} \gamma_k n_k \left( \sum_{j=0}^{J-1} \beta_{k,j} x_j \right) \quad (3)$$

<sup>129</sup> where  $\mu_0$  is a global bias for  $K$  individually specified ANN subnetworks,  $n_k$ , with weights  $\gamma_k$ . The  
<sup>130</sup> inputs to each  $n_k$  are themselves a linear combination of the  $J$  modeling inputs and their associated  
<sup>131</sup>  $\beta_{k,j}$  coefficients in the deepest, i.e., *projection*, layer of  $g^{\text{XNN}}$ .

<sup>132</sup> Two  $g^{\text{XNN}}$  models are trained by mini-batch stochastic gradient descent (SGD) on the simulated  
<sup>133</sup> data and mortgage data. Each  $g^{\text{XNN}}$  is assessed in 5 training folds and in a test data partition.  $L_1$   
<sup>134</sup> regularization is applied to network weights to induce a sparse and interpretable model, where each  
<sup>135</sup>  $n_k$  and corresponding  $\gamma_k$  are ideally associated with an important  $X_j$  or combination thereof. The  $g^{\text{XNN}}$   
<sup>136</sup> models appear highly sensitive to weight initialization and batch size. Be aware that  $g^{\text{XNN}}$  model  
<sup>137</sup> architectures may require manual and judicious feature selection due to long training times. For more  
<sup>138</sup> details regarding  $g^{\text{XNN}}$  training, see the software resources in Subsection [1.8](#) and Appendices [B.1](#) and  
<sup>139</sup> [B.3](#).

#### <sup>140</sup> 1.5. One-dimensional Partial Dependence and Individual Conditional Expectation

<sup>141</sup> PD plots are a widely-used method for describing and plotting the estimated average prediction  
<sup>142</sup> of a complex model,  $g$ , across some partition of data,  $\mathbf{X}$ , for some interesting input feature,  $X_j \in \mathbf{X}$   
<sup>143</sup> [13]. ICE plots are a newer method that describes the local behavior of  $g$  with regard to values of an  
<sup>144</sup> input feature in a single instance,  $x_j$ . PD and ICE can be overlaid in the same plot to create a holistic  
<sup>145</sup> global and local portrait of the predictions for some  $g$  and  $X_j$  [22]. When  $\text{PD}(X_j, g)$  and  $\text{ICE}(x_j, g)$   
<sup>146</sup> curves diverge, such plots can also be indicative of modeled interactions in  $g$  or expose flaws in PD  
<sup>147</sup> estimation, e.g., inaccuracy in the presence of strong interactions and correlations [22], [29]. For details

<sup>148</sup> regarding the calculation of one-dimensional PD and ICE, see the software resources in Subsection 1.8  
<sup>149</sup> and Appendices B.1 and B.4.

<sup>150</sup> 1.6. *Shapley Values*

<sup>151</sup> Shapley explanations are a class of additive, locally accurate feature contribution measures with  
<sup>152</sup> long-standing theoretical support [23], [30]. Shapley explanations are the only known locally accurate  
<sup>153</sup> and globally consistent feature contribution values, meaning that Shapley explanation values for input  
<sup>154</sup> features always sum to the model's prediction,  $g(\mathbf{x})$ , for any instance  $\mathbf{x}$ , and that Shapley explanation  
<sup>155</sup> values should not decrease in magnitude for some instance of  $x_j$  when  $g$  is changed such that  $x_j$   
<sup>156</sup> truly makes a stronger contribution to  $g(\mathbf{x})$  [23], [24]. Shapley values can be estimated in different  
<sup>157</sup> ways, many of which are intractable for datasets with large numbers of input features. Tree SHAP  
<sup>158</sup> (SHapley Additive exPlanations) is a specific implementation of Shapley explanations that relies  
<sup>159</sup> on traversing internal decision tree structures to efficiently estimate the contribution of each  $x_j$  for  
<sup>160</sup> some  $g(\mathbf{x})$  [24]. Tree SHAP has been implemented in popular gradient boosting libraries such as  
<sup>161</sup> [h2o](#), [LightGBM](#), and [XGBoost](#), and Tree SHAP is used to calculate accurate and consistent global and  
<sup>162</sup> local feature importance for MGBM models in Subsection 2.2.2 and Appendix E.1. Deep SHAP is  
<sup>163</sup> an approximate Shapley value technique that creates SHAP values for ANNs [23]. Deep SHAP is  
<sup>164</sup> implemented in the [shap](#) package and is used to generate SHAP values for the two  $g^{XNN}$  models  
<sup>165</sup> discussed in Subsection 2.2.2 and Appendix E.1. For more information pertaining to the calculation of  
<sup>166</sup> Shapley values, see Appendices B.1 and B.5.

<sup>167</sup> 1.7. *Discrimination Testing Measures*

<sup>168</sup> Because many current technical discussions of fairness in ML appear inconclusive<sup>8</sup>, this text  
<sup>169</sup> will draw on regulatory and legal standards that have been used for years in regulated, high-stakes  
<sup>170</sup> employment and financial decisions. The discussed measures are also representative of fair lending  
<sup>171</sup> analyses and pair well with the mortgage data. See Appendix C for a brief discussion regarding  
<sup>172</sup> different types of discrimination in US legal and regulatory settings and Appendix D for remarks on  
<sup>173</sup> practical vs. statistical significance for discrimination measures. One such common measure of DI  
<sup>174</sup> used in US litigation and regulatory settings is ME. ME is simply the difference between the percent  
<sup>175</sup> of the control group members receiving a favorable outcome and the percent of the protected class  
<sup>176</sup> members receiving a favorable outcome.

$$\text{ME} \equiv 100 \cdot (\Pr(\hat{\mathbf{y}} = 1 | X_c = 1) - \Pr(\hat{\mathbf{y}} = 1 | X_p = 1)) \quad (4)$$

<sup>177</sup> where  $\hat{\mathbf{y}}$  are the model decisions,  $X_p$  and  $X_c$  represent binary markers created from some demographic  
<sup>178</sup> attribute,  $c$  denotes the control group (often whites or males),  $p$  indicates a protected group, and  $\Pr(\cdot)$   
<sup>179</sup> is the operator for conditional probability. ME is a favored DI measure used by the US Consumer  
<sup>180</sup> Financial Protection Bureau (CFPB), the primary agency charged with regulating fair lending laws at  
<sup>181</sup> the largest US lending institutions and for various other participants in the consumer financial market.<sup>9</sup>  
<sup>182</sup> Another important DI measure is AIR, more commonly known as a *relative risk ratio* in settings outside  
<sup>183</sup> of regulatory compliance.

$$\text{AIR} \equiv \frac{\Pr(\hat{\mathbf{y}} = 1 | X_p = 1)}{\Pr(\hat{\mathbf{y}} = 1 | X_c = 1)} \quad (5)$$

<sup>184</sup> AIR is equal to the ratio of the proportion of the protected class that receives a favorable outcome and  
<sup>185</sup> the proportion of the control class that receives a favorable outcome. Statistically significant AIR values

---

<sup>8</sup> See: [Tutorial: 21 Fairness Definitions and Their Politics](#).

<sup>9</sup> See: [Supervisory Highlights, Issue 9, Fall 2015](#).

below 0.8 can be considered *prima facia* evidence of discrimination. An additional long-standing and pertinent measure of DI is SMD. SMD is often used to assess disparities in continuous features, such as income differences in employment analyses, or interest rate differences in lending. It originates from work on statistical power, and is more formally known as *Cohen's d*. SMD is equal to the difference in the average protected class outcome,  $\bar{y}_p$ , minus the control class outcome,  $\bar{y}_c$ , divided by a measure of the standard deviation of the population,  $\sigma_{\bar{y}}$ .<sup>10</sup> Cohen defined values of this measure to have *small*, *medium*, and *large* effect sizes if the values exceeded 0.2, 0.5, and 0.8, respectively.

$$\text{SMD} \equiv \frac{\bar{y}_p - \bar{y}_c}{\sigma_{\bar{y}}} \quad (6)$$

The numerator in the SMD is roughly equivalent to ME but adds the standard deviation divisor as a standardizing factor. Because of this standardization factor, SMD allows for a comparison across different types of outcomes, such as inequity in mortgage closing fees or inequities in the interest rates given on certain loans. In this, one may apply definitions in Cohen [25] of *small*, *medium*, and *large* effect sizes, which represent a measure of *practical significance*, which is described in detail in Appendix D. Finally, confusion matrix measures in demographic groups, such as accuracy, false positive rate (FPR), false negative rate (FNR), and their ratios, are also considered as measures of DI in Subsection 2.2.3 and Appendix E.2.

### 1.8. Software Resources

Python code to reproduce discussed results is available at: <https://github.com/h2oai/article-information-2019>. The primary Python packages employed are: `numpy` and `pandas` for data manipulation, `h2o`, `keras`, `shap`, and `tensorflow` for modeling, explanation, and discrimination testing, and typically `matplotlib` for plotting.

## 2. Results

Results are laid out for the simulated and mortgage datasets. Accuracy is compared for unconstrained, less interpretable  $g^{\text{GBM}}$  and  $g^{\text{ANN}}$  models and constrained, more interpretable  $g^{\text{MGBM}}$  and  $g^{\text{XNN}}$  models. Then, for the  $g^{\text{MGBM}}$  and  $g^{\text{XNN}}$  models, intrinsic interpretability, post-hoc explanation, and discrimination testing results are explored.

### 2.1. Simulated Data Results

Fit comparisons between unconstrained and constrained models and XNN interpretability results are discussed in Subsections 2.1.1 and 2.1.2. As model training and assessment on the simulated data is a rough validation exercise meant to showcase expected results on data with known characteristics, and given that most of the techniques in the proposed workflow are already used widely or have been validated elsewhere, reporting of simulated data results in the main text will focus mostly on fit measures and the more novel  $g^{\text{XNN}}$  interpretability results. The bulk of the post-hoc explanation and discrimination testing results for the simulated data are left to Appendix E.

#### 2.1.1. Constrained vs. Unconstrained Model Fit Assessment

Table 1 presents a variety of fit measures for  $g^{\text{GBM}}$ ,  $g^{\text{MGBM}}$ ,  $g^{\text{ANN}}$ , and  $g^{\text{XNN}}$  on the simulated test data.  $g^{\text{XNN}}$  exhibits the best performance, but the models exhibit only a fairly small range of fit results. Interpretability and explainability benefits of the constrained models appear to come at little cost to

<sup>10</sup> There are several measures of the standard deviation of the score that are typically used: 1. the standard deviation of the population, irrespective of protected class status, 2. a standard deviation calculated only over the two groups being considered in a particular calculation, or 3. a pooled standard deviation, using the standard deviations for each of the two groups with weights.

overall model performance, or in the case of  $g^{\text{ANN}}$  and  $g^{\text{XNN}}$ , no cost at all. For the displayed measures,  $g^{\text{MGBM}}$  performs  $\sim 2\%$  worse on average than  $g^{\text{GBM}}$ .  $g^{\text{XNN}}$  performs  $\sim 0.5\%$  better on average than  $g^{\text{XNN}}$ , and  $g^{\text{XNN}}$  actually shows slightly better fit than  $g^{\text{ANN}}$  across all fit measures except specificity. Fit measures that require a probability cutoff are taken at the best F1 threshold for each model.

**Table 1.** Fit measures for  $g^{\text{GBM}}(\mathbf{X})$ ,  $g^{\text{MGBM}}(\mathbf{X})$ ,  $g^{\text{ANN}}(\mathbf{X})$ , and  $g^{\text{XNN}}(\mathbf{X})$  on the simulated test data. Arrows indicate the direction of improvement for each measure.

Model	Accuracy $\uparrow$	AUC $\uparrow$	F1 $\uparrow$	Logloss $\downarrow$	MCC $\uparrow$	RMSE $\downarrow$	Sensitivity $\uparrow$	Specificity $\uparrow$
$g^{\text{GBM}}$	0.757	0.847	0.779	0.486	0.525	0.400	0.858	0.657
$g^{\text{MGBM}}$	0.744	0.842	0.771	0.502	0.504	0.407	0.864	0.625
$g^{\text{ANN}}$	0.757	0.850	0.779	0.480	0.525	0.398	0.858	0.657
$g^{\text{XNN}}$	0.758	0.851	0.781	0.479	0.528	0.397	0.867	0.648

### 2.1.2. Interpretability Results

For  $g^{\text{XNN}}$ , inherent interpretability manifests as plots of sparse  $\gamma_k$  output layer weights,  $n_k$  subnetwork ridge functions, and sparse  $\beta_{j,k}$  weights in the bottom projection layer. Figure 1 provides detailed insights into the structure of  $g^{\text{XNN}}$  (also described in Equation 3). 1a displays the sparse  $\gamma_k$  weights of the output layer, where only  $n_k$  subnetworks with  $k \in \{1, 4, 7, 8, 9\}$  are associated with large magnitude weights. The  $n_k$  subnetwork ridge functions appear in 1b as simplistic but distinctive functional forms. Color-coding between 1a and 1b visually reinforces the direct feed-forward relationship between the  $n_k$  subnetworks and the  $\gamma_k$  weights of the output layer.

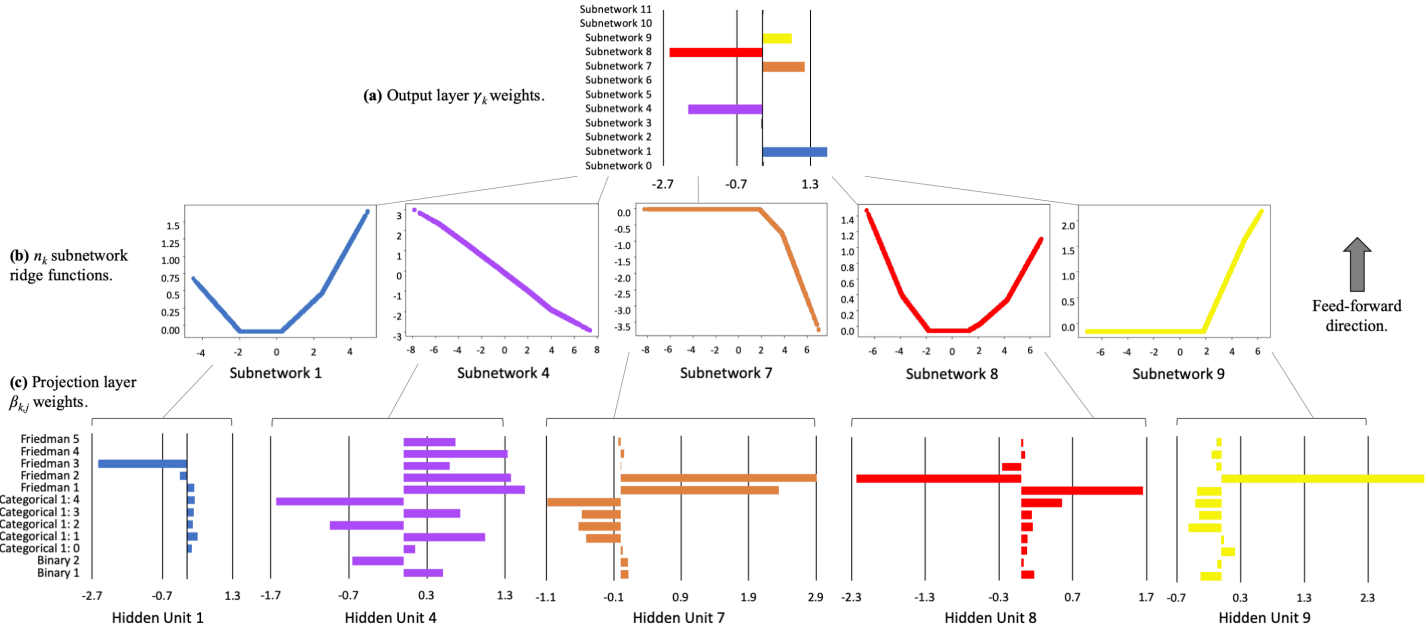


**Figure 1.** Output layer  $\gamma_k$  weights, corresponding  $n_k$  subnetwork ridge functions, and associated projection layer  $\beta_{k,j}$  weights for  $g^{\text{XNN}}$  on the simulated data.

$n_k$  subnetworks are plotted across the output values of their associated  $\sum_j \beta_{k,j} x_j$  projection layer hidden units, and color-coding between 1b and 1c link the  $\beta_{j,k}$  weights to their  $n_k$  subnetworks. Most of the heavily utilized  $n_k$  subnetworks have sparse weights in their  $\sum_j \beta_{k,j} x_j$  projection layer hidden units. In particular, subnetwork  $n_1$  appears to be almost solely a function of  $X_{\text{Friedman},3}$  and appears to exhibit the expected quadratic behavior for  $X_{\text{Friedman},3}$ . Subnetworks  $n_7$ ,  $n_8$ , and  $n_9$  appear to be most associated with the globally important  $X_{\text{Friedman},1}$  and  $X_{\text{Friedman},2}$  features, likely betraying the effort required for  $g^{\text{XNN}}$  to model the nonlinear  $\sin()$  function of the  $X_{\text{Friedman},1}$  and  $X_{\text{Friedman},2}$  product, and

these subnetworks, especially  $n_7$  and  $n_8$ , appear to display some noticeable sinusoidal characteristics. Subnetwork  $n_4$  seems to be a linear combination of all the original input  $X_j$  features, but does weigh the linear  $X_{\text{Friedman},4}$  and  $X_{\text{Friedman},5}$  terms roughly in the correct two-to-one ratio. As a whole, Figure 1a, b, and c exhibit evidence that  $g^{\text{XNN}}$  has learned about the signal-generating function in Equation 1 and the displayed information should help practitioners understand which original input  $X_j$  features are weighed heavily in each  $n_k$  subnetwork, and which  $n_k$  subnetworks have a strong influence on  $g^{\text{XNN}}(\mathbf{X})$  output. See Appendix B.3 for additional details regarding general XNN architecture.

## 2.2. Mortgage Data Results

Results for the mortgage data are presented in Subsections 2.2.1 – 2.2.3 to showcase the example workflow.  $g^{\text{ANN}}$  and  $g^{\text{XNN}}$  outperform  $g^{\text{GBM}}$  and  $g^{\text{MGBM}}$  on the mortgage data, but as in Subsection 2.1.1 the constrained variants of both model architectures do not show large differences in model fit with respect to unconstrained variants. Assuming that in high-stakes applications small fit differences on static test data do not outweigh the need for enhanced model debugging facilitated by high interpretability, only  $g^{\text{MGBM}}$  and  $g^{\text{XNN}}$  interpretability, post-hoc explainability, and discrimination testing results are presented.

### 2.2.1. Constrained vs. Unconstrained Model Fit Assessment

Table 2 shows that  $g^{\text{ANN}}$  and  $g^{\text{XNN}}$  noticeably outperform  $g^{\text{GBM}}$  and  $g^{\text{MGBM}}$  on the mortgage data for most of the fit measures. This is at least partially due to the preprocessing required to present directly comparable post-hoc explainability results and to use neural networks and tensorflow, e.g., numerical encoding of categorical features and missing values. This preprocessing appears to hamstring some of the tree-based models' inherent capabilities.  $g^{\text{GBM}}$  models trained on non-encoded data with missing values repeatedly produced area under the curve (AUC) values of  $\sim 0.81$  (not shown, but available in resources discussed in Subsection 1.8).

**Table 2.** Fit measures for  $g^{\text{GBM}}(\mathbf{X})$ ,  $g^{\text{MGBM}}(\mathbf{X})$ ,  $g^{\text{ANN}}(\mathbf{X})$ , and  $g^{\text{XNN}}(\mathbf{X})$  on the mortgage test data. Arrows indicate the direction of improvement for each measure.

Model	Accuracy ↑	AUC ↑	F1 ↑	Logloss ↓	MCC ↑	RMSE ↓	Sensitivity ↑	Specificity ↑
$g^{\text{GBM}}$	0.795	0.828	0.376	0.252	0.314	0.276	0.634	0.813
$g^{\text{MGBM}}$	0.765	0.814	0.362	0.259	0.305	0.278	0.684	0.773
$g^{\text{ANN}}$	0.865	0.871	0.474	0.231	0.418	0.262	0.624	0.891
$g^{\text{XNN}}$	0.869	0.868	0.468	0.233	0.409	0.263	0.594	0.898

Regardless of the fit differences between the two families of models, the difference between the constrained and unconstrained variants within the two types of models is small for the GBMs and smaller for the ANNs,  $\sim 3.5\%$  and  $\sim 1\%$  worse fit respectively, averaged across the measures in Table 2.

### 2.2.2. Interpretability and Post-hoc Explanation Results

For  $g^{\text{MGBM}}(\mathbf{X})$ , intrinsic interpretability is evaluated with PD and ICE plots of mostly monotonic prediction behavior for several important  $X_j$ , and post-hoc Shapley explanation analysis is used to create global and local feature importance. Global Shapley feature importance for  $g^{\text{MGBM}}(\mathbf{X})$  on the mortgage test data is reported in Figure 2.  $g^{\text{MGBM}}$  places high importance on LTV ratio, perhaps too high, and also weighs DTI ratio, property value, loan amount, and introductory rate period heavily in many of its predictions. Tree SHAP values are reported in the margin space, prior to the application of the logit link function, and the reported numeric values can be interpreted as the mean absolute impact of each  $X_j$  on  $g^{\text{MGBM}}(\mathbf{X})$  in the mortgage test data in the  $g^{\text{MGBM}}(\mathbf{X})$  margin space. The potential over-emphasis of LTV ratio, and the de-emphasis of income, likely an important feature from a business

<sup>278</sup> perspective, and the de-emphasis of the encoded no introductory rate period flag feature may also  
<sup>279</sup> contribute to the decreased performance of  $g^{\text{MGBM}}(\mathbf{X})$  as compared to  $g^{\text{XNN}}(\mathbf{X})$ .

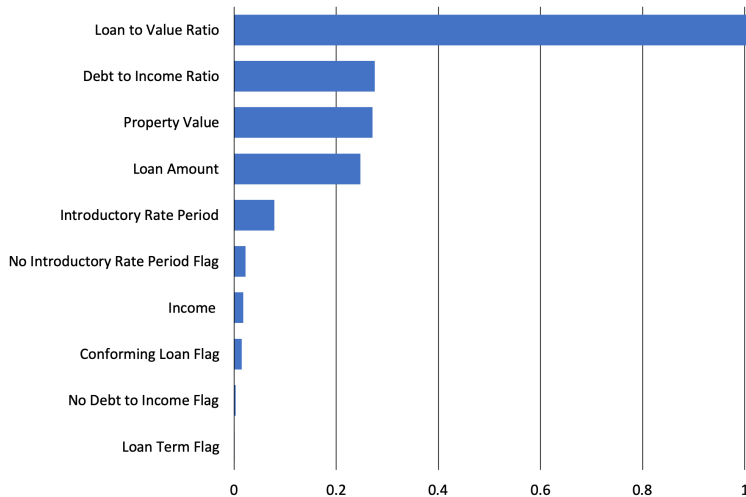


**Figure 2.** Global mean absolute Tree SHAP feature importance for  $g^{\text{MGBM}}(\mathbf{X})$  on the mortgage test data.

<sup>280</sup> Domain knowledge was used to positively constrain DTI ratio and LTV ratio and to negatively  
<sup>281</sup> constrain income and the loan term flag under  $g^{\text{MGBM}}$ . The monotonicity constraints for DTI ratio  
<sup>282</sup> and LTV ratio are confirmed for  $g^{\text{MGBM}}(\mathbf{X})$  on the mortgage test data in Figure 3. Both DTI ratio and  
<sup>283</sup> LTV ratio display positive monotonic behavior at all selected percentiles of  $g^{\text{MGBM}}(\mathbf{X})$  for ICE and on  
<sup>284</sup> average with PD. Because PD curves generally follow the patterns of the ICE curves for both features,  
<sup>285</sup> it's also likely that no strong interactions are at play for DTI ratio and LTV ratio under  $g^{\text{MGBM}}$ . Of  
<sup>286</sup> course, the monotonicity constraints themselves can dampen the effects of non-monotonic interactions  
<sup>287</sup> under  $g^{\text{MGBM}}$ , even if they do exist in the training data (e.g., LTV ratio and the no introductory rate  
<sup>288</sup> period flag, see Figure 6). This rigidity could also play a role in the performance differences between  
<sup>289</sup>  $g^{\text{MGBM}}(\mathbf{X})$  and  $g^{\text{XNN}}(\mathbf{X})$  in the mortgage data not observed for the simulated data, wherein strong  
<sup>290</sup> interactions appear to be between features with the same monotonicity constraints (e.g.,  $X_{\text{Friedman},1}$   
<sup>291</sup> and  $X_{\text{Friedman},2}$ , see Figure 1).

<sup>292</sup> PD and ICE are displayed with a histogram to highlight any sparse regions in an input feature's  
<sup>293</sup> domain. Because most ML models will always issue a prediction on any instance with a correct schema,  
<sup>294</sup> it's crucial to consider whether a given model learned enough about an instance to make an accurate  
<sup>295</sup> prediction. Viewing PD and ICE along with a histogram is a convenient method to visually assess  
<sup>296</sup> whether a prediction is reasonable and based on sufficient training data. DTI ratio and LTV ratio do  
<sup>297</sup> appear to have sparse regions in their univariate distributions. The monotonicity constraints likely  
<sup>298</sup> play to the advantage of  $g^{\text{MGBM}}$  in this regard, as  $g^{\text{MGBM}}(\mathbf{X})$  appears to carry reasonable predictions  
<sup>299</sup> learned from dense domains into the sparse domains of both features.

<sup>300</sup> Figure 3 also displays PD and ICE for the unconstrained feature property value. Unlike DTI ratio  
<sup>301</sup> and LTV ratio, PD for property value does not always follow the patterns established by ICE curves.  
<sup>302</sup> While PD shows monotonically increasing prediction behavior on average, apparently influenced by  
<sup>303</sup> large predictions at extreme  $g^{\text{MGBM}}(\mathbf{X})$  percentiles, ICE curves for individuals at the 40<sup>th</sup> percentile  
<sup>304</sup> of  $g^{\text{MGBM}}(\mathbf{X})$ , and lower, exhibit different prediction behavior with respect to property value. Some  
<sup>305</sup> individuals at these lower percentiles display monotonically decreasing prediction behavior while  
<sup>306</sup> others appear to show fluctuating prediction behavior. Property value is strongly right-skewed, with  
<sup>307</sup> little data regarding high-value property from which  $g^{\text{MGBM}}$  can learn. For the most part, reasonable  
<sup>308</sup> predictions do appear to be carried from more densely populated regions to more sparsely populated  
<sup>309</sup> regions. However, prediction fluctuations at lower  $g^{\text{MGBM}}(\mathbf{X})$  percentiles are visible, and appear in a  
<sup>310</sup> sparse region of property value. This divergence of PD and ICE can be indicative of an interaction  
<sup>311</sup> affecting property value under  $g^{\text{MGBM}}$  [22], and analysis by surrogate decision tree did show evidence

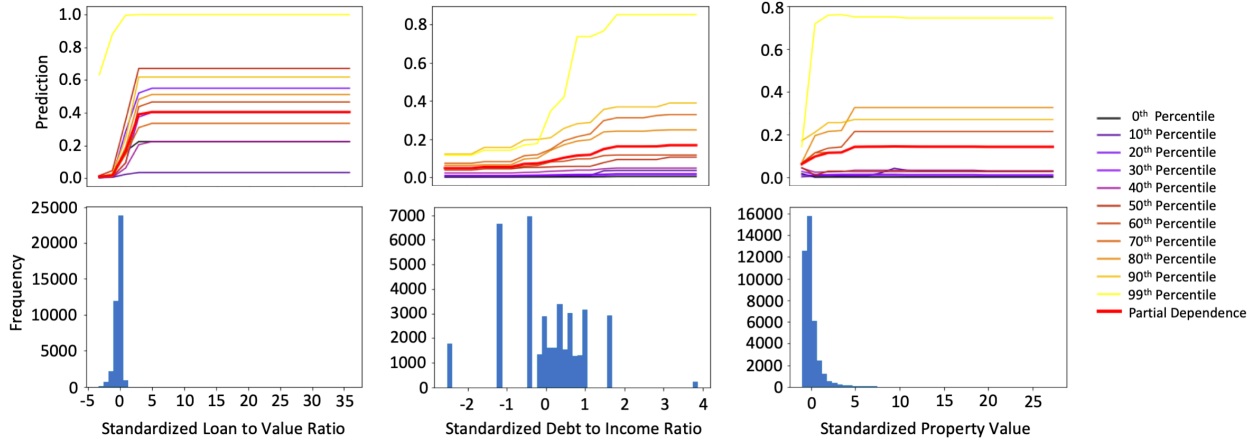


**Figure 3.** PD, ICE for 10 individuals across selected percentiles of  $g^{\text{MGBM}}(\mathbf{X})$ , and histograms for the three most important input features of  $g^{\text{MGBM}}$  on the mortgage test data.

of numerous potential interactions in lower predictions ranges of  $g^{\text{MGBM}}(\mathbf{X})$  [31] (not shown, but available in resources discussed in Subsection 1.8). Fluctuations in ICE could also be caused by overfitting or by leakage of strong non-monotonic signal from important constrained features into the modeled behavior of non-constrained features.

In Figure 4, local Tree SHAP values are displayed for selected individuals at the 10<sup>th</sup>, 50<sup>th</sup>, and 90<sup>th</sup> percentiles of  $g^{\text{MGBM}}(\mathbf{X})$  in the mortgage test data. Each Shapley value in Figure 4 represents the difference in  $g^{\text{MGBM}}(\mathbf{x})$  and the average of  $g^{\text{MGBM}}(\mathbf{X})$  associated with this instance of some input feature  $x_j$  [32]. Accordingly, the logit of the sum of the Shapley values and the average of  $g^{\text{MGBM}}(\mathbf{X})$  is  $g^{\text{MGBM}}(\mathbf{x})$ , the prediction in the probability space for any  $\mathbf{x}$ .

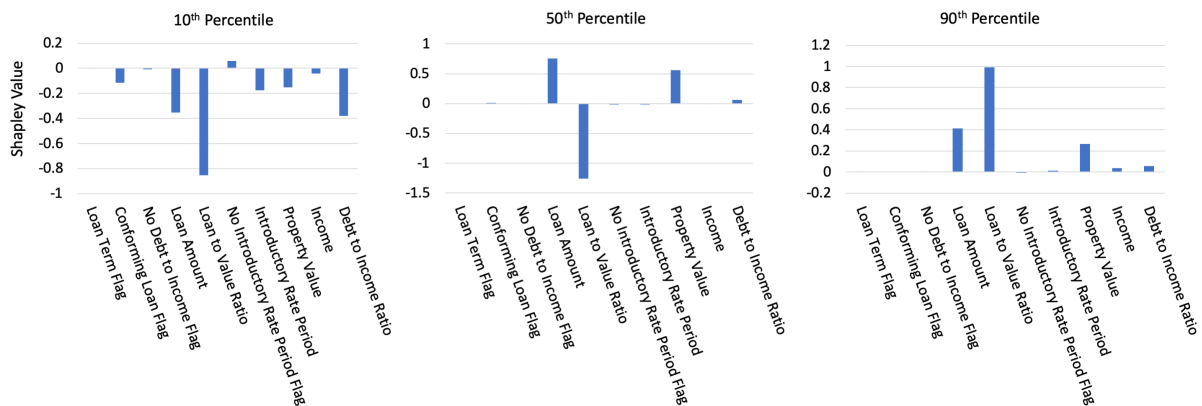


**Figure 4.** Tree SHAP values for three individuals across selected percentiles of  $g^{\text{MGBM}}(\mathbf{X})$  for the mortgage test data.

The selected individuals show an expected progression of mostly negative Shapley values at the 10<sup>th</sup> percentile, a mixture of positive and negative Shapley values at the 50<sup>th</sup> percentile, mostly positive Shapley values the 90<sup>th</sup> percentile, and with globally important features driving most local model decisions. Deeper significance for Figure 4 lies in the ability of Tree SHAP to accurately and consistently summarize any single  $g^{\text{MGBM}}(\mathbf{x})$  prediction in this manner, which is generally important for enabling logical appeal or override of ML-based decisions, and is specifically important in the context of lending, where applicable regulations often require lenders to provide consumer-specific reasons for denying credit to an individual. In the US, applicable regulations are typically ECOA and FCRA, and the consumer-specific reasons are commonly known as *adverse actions codes*.

Figure 5 displays global feature importance for  $g^{\text{XNN}}(\mathbf{X})$  on the mortgage test data. Deep SHAP values are reported in the probability space, after the application of the logit link function. They are

332 also calculated from the projection layer of  $g^{XNN}$ . Thus, the Deep SHAP values in Figure 5 are the  
 333 estimated average absolute impact of each input,  $X_j$ , in the projection layer and probability space of  
 334  $g^{XNN}(\mathbf{X})$  for the mortgage test data.  $g^{XNN}$  distributes importance more evenly across business drivers  
 335 and puts stronger emphasis on the no introductory rate period flag feature than does  $g^{MGBM}$ . Like  
 336  $g^{MGBM}$ ,  $g^{XNN}$  puts little emphasis on the other flag features.

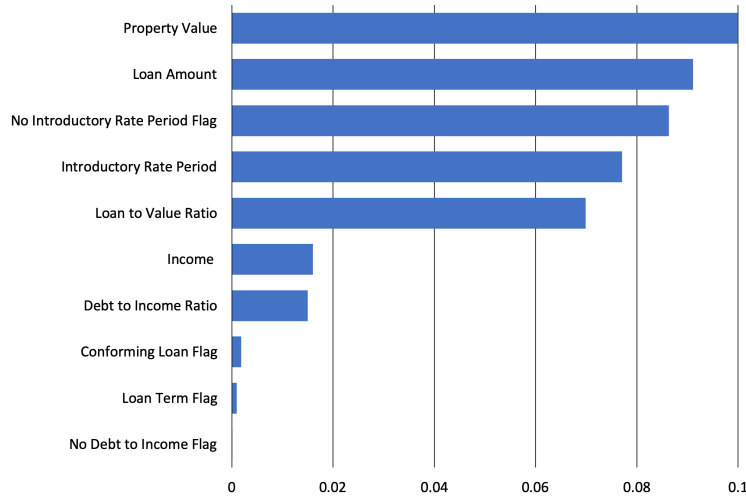


Figure 5. Global mean absolute Deep SHAP feature importance for  $g^{XNN}(\mathbf{X})$  on the mortgage test data.

337 As compared to  $g^{MGBM}$ ,  $g^{XNN}$  assigns higher importance to property value, loan amount, and income,  
 338 and lower importance on LTV ratio and DTI ratio.

339 The capability of  $g^{XNN}$  to model nonlinear phenomenon and high-degree interactions, and to do  
 340 so in an interpretable manner, is on display in Figure 6. 6a presents the sparse  $\gamma_k$  weights of the  $g^{XNN}$   
 341 output layer in which the  $n_k$  subnetworks with  $k \in \{0, 1, 2, 3, 5, 8, 9\}$  have large magnitude weights and  
 342  $n_k$  subnetworks,  $k \in \{4, 6, 7\}$ , have small or near-zero magnitude weights. Distinctive ridge functions  
 343 that feed into those large magnitude  $\gamma_k$  weights are highlighted in 6b and color-coded to pair with  
 344 their corresponding  $\gamma_k$  weight. As in the Subsection 2.1.2,  $n_k$  ridge function plots vary with the output  
 345 of the corresponding projection layer  $\sum_j \beta_{k,j} x_j$  hidden unit, with weights displayed in matching colors  
 346 in 6c. In both the simulated and mortgage data,  $n_k$  ridge functions appear to be elementary functional  
 347 forms that the output layer learns to combine to generate accurate predictions, reminiscent of basis  
 348 functions for the modeled space. 6c displays the sparse  $\beta_{j,k}$  weights of the projection layer  $\sum_j \beta_{k,j} x_j$   
 349 hidden units that are associated with each  $n_k$  subnetwork ridge function. For instance, subnetwork  
 350  $n_3$  is influenced by large weights for LTV ratio, no introductory rate period flag, and introductory  
 351 rate period, whereas subnetwork  $n_9$  is nearly completely dominated by the weight for income. See  
 352 Appendix B.3 for details regarding general XNN architecture.

353 To compliment the global interpretability of  $g^{XNN}$ , Figure 7 displays local Shapley values for  
 354 selected individuals, estimated from the projection layer using Deep SHAP in the  $g^{XNN}$  probability  
 355 space. Similar to Tree SHAP, local Deep SHAP values should sum to  $g^{XNN}(\mathbf{x})$ . While the Shapley  
 356 values appear to follow the roughly increasing pattern established in Figures A4, A6, and 4, their true  
 357 value is their ability to be calculated for any  $g^{XNN}(\mathbf{x})$  prediction, as a means to summarize model  
 358 reasoning and allow for appeal and override of specific ML-based decisions.

### 359 2.2.3. Discrimination Testing Results

360 Tables 3a and 3b show the results of the discrimination tests using the mortgage data for two sets  
 361 of class-control groups: blacks as compared to whites, and females as compared to males. As with  
 362 the simulated data in Table A1, several measures of disparities are shown, with the SMDs calculated  
 363 using the probabilities from  $g^{MGBM}(\mathbf{X})$  and  $g^{XNN}(\mathbf{X})$ , and the accuracy, FPRs, and FPR ratios, MEs,  
 364 and AIRs calculated using a binary outcome based on a cutoff of 0.20 (anyone with probabilities of

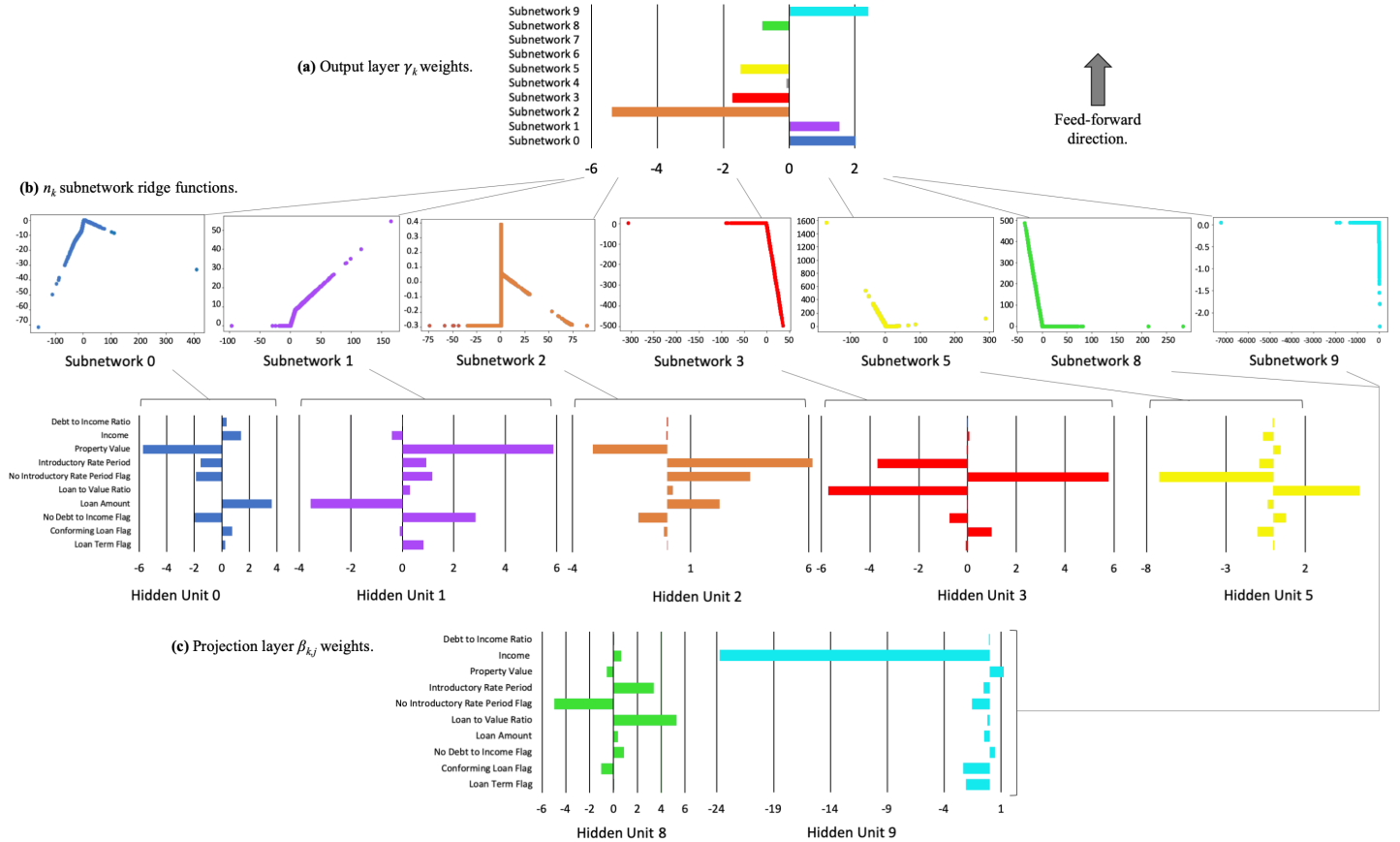


**Figure 6.** Output layer  $\gamma_k$  weights, corresponding  $n_k$  ridge functions, and associated projection layer  $\beta_{k,j}$  weights for  $g^{\text{XNN}}$  on the mortgage data.

0.2 or less receives the favorable outcome).<sup>11</sup> Since  $g^{\text{MGBM}}$  and  $g^{\text{XNN}}$  are predicting the likelihood of receiving a high-priced loan,  $g^{\text{MGBM}}$  and  $g^{\text{XNN}}$  assume that a lower score is favorable. Thus, one might consider FPR ratios as a measure of the class-control disparities. FPR ratios are higher under  $g^{\text{XNN}}$  than  $g^{\text{MGBM}}$  (2.45 vs. 2.10) in Table 3b, but overall FPRs are lower for blacks under  $g^{\text{XNN}}$  (0.295 vs. 0.315) in Table 3a. This is the same pattern seen in the simulated data results in Appendix E.2, leading to the question of whether a fairness goal should not only consider class-control relative rates, but also intra-class improvements in the chosen fairness measure. Similar results are found for the female-male comparison, but the relative rates are less stark: 1.15 for  $g^{\text{MGBM}}(\mathbf{X})$  and 1.21 for  $g^{\text{XNN}}(\mathbf{X})$ .

Both ME and AIR show higher disparities for blacks under  $g^{\text{XNN}}$  than  $g^{\text{MGBM}}$ . Blacks receive high-priced loans 21.4% more frequently using  $g^{\text{XNN}}$  vs. 18.3% for  $g^{\text{MGBM}}$ . Both  $g^{\text{MGBM}}$  and  $g^{\text{XNN}}$  show AIRs that are statistically significantly below parity (not shown, but available in resources discussed in Subsection 1.8), and which are also below the EEOC's 0.80 threshold. This would typically indicate need for further review to determine the cause and validity of these disparities, and a few relevant remediation techniques for such discovered discrimination are discussed in Subsection 3.3. On the other hand, women improve under  $g^{\text{XNN}}$  vs.  $g^{\text{MGBM}}$  (MEs of 3.6% vs. 4.1%; AIRs of 0.955 vs. 0.948). The AIRs, while statistically significantly below parity, are well above the EEOC's threshold of 0.80. In most situations, the values of these measures alone would not likely flag a model for further review. Black SMDs for  $g^{\text{XNN}}(\mathbf{X})$  and  $g^{\text{MGBM}}(\mathbf{X})$  are similar: 0.621 and 0.628, respectively. These exceed Cohen's guidelines of 0.5 for a medium effect size and would likely trigger further review.

<sup>11</sup> See Appendix F for comments pertaining to discrimination testing and cutoff selection.

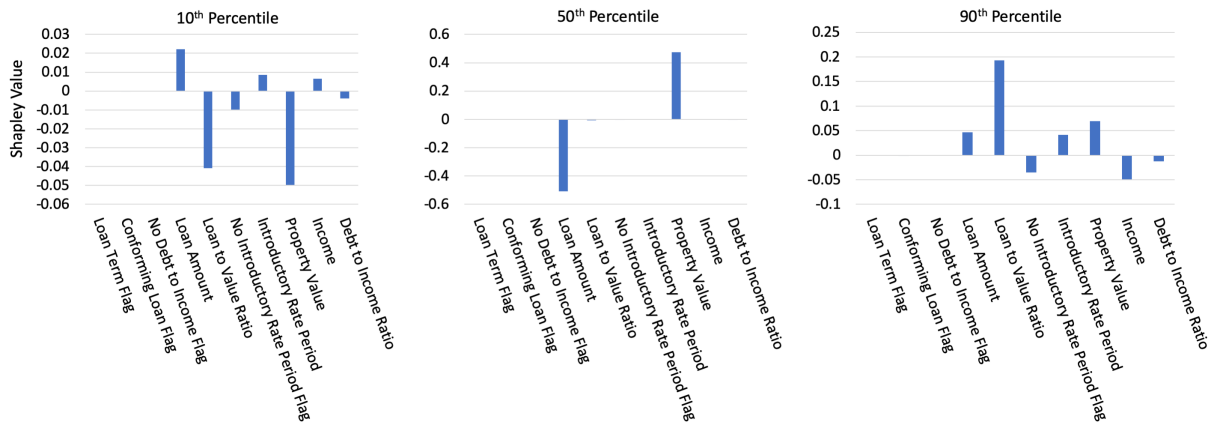


**Figure 7.** Deep SHAP values for three individuals across selected percentiles of  $g^{XNN}(X)$  on the mortgage test data.

(a) Group size, accuracy, and FPR for  $g^{MGBM}(X)$  and  $g^{XNN}(X)$  on the mortgage test data.

Class	N	Model	Accuracy↑	FPR↓
Black	2,608	$g^{MGBM}$	0.654	0.315
		$g^{XNN}$	0.702	0.295
White	28,361	$g^{MGBM}$	0.817	0.150
		$g^{XNN}$	0.857	0.120
Female	8,301	$g^{MGBM}$	0.768	0.208
		$g^{XNN}$	0.822	0.158
Male	13,166	$g^{MGBM}$	0.785	0.182
		$g^{XNN}$	0.847	0.131

(b) AIR, ME, SMD, and FPR ratio for  $g^{MGBM}(X)$  and  $g^{XNN}(X)$  on the mortgage test data.

Model	Protected Class	Control Class	AIR↑	ME↓	SMD↓	FPR Ratio↓
$g^{MGBM}$	Black	White	0.776	18.3%	0.628	2.10
	Female	Male	0.948	4.1%	0.084	1.15
$g^{XNN}$	Black	White	0.743	21.4%	0.621	2.45
	Female	Male	0.955	3.6%	0.105	1.21

**Table 3.** Discrimination measures for the mortgage test data. Arrows indicate the direction of improvement for each measure.

384 Female SMDs are well below Cohen's definition of small effect size: 0.105 and 0.084 for  $g^{XNN}(X)$  and  
 385  $g^{MGBM}(X)$ , respectively. Similar to results for female AIR, these values alone are unlikely to prompt  
 386 further review.

### 3. Discussion

#### 3.1. The Burgeoning Python Ecosystem for Responsible Machine Learning

389 Figure 8 displays a holistic approach to ML model training, assessment, and deployment meant  
 390 to decrease discrimination, inaccuracy, privacy, and security risks for high-stakes, human-centered, or  
 391 regulated ML applications.<sup>12</sup> While all the methods mentioned in Figure 8 play an important role in  
 392 increasing human trust and understanding of ML, a few pertinent references and Python resources are  
 393 highlighted below as further reading to augment this text's focus on certain interpretable models,  
 394 post-hoc explanation, and discrimination testing techniques.

<sup>12</sup> See: [Toward Responsible Machine Learning](#) for details regarding Figure 8.

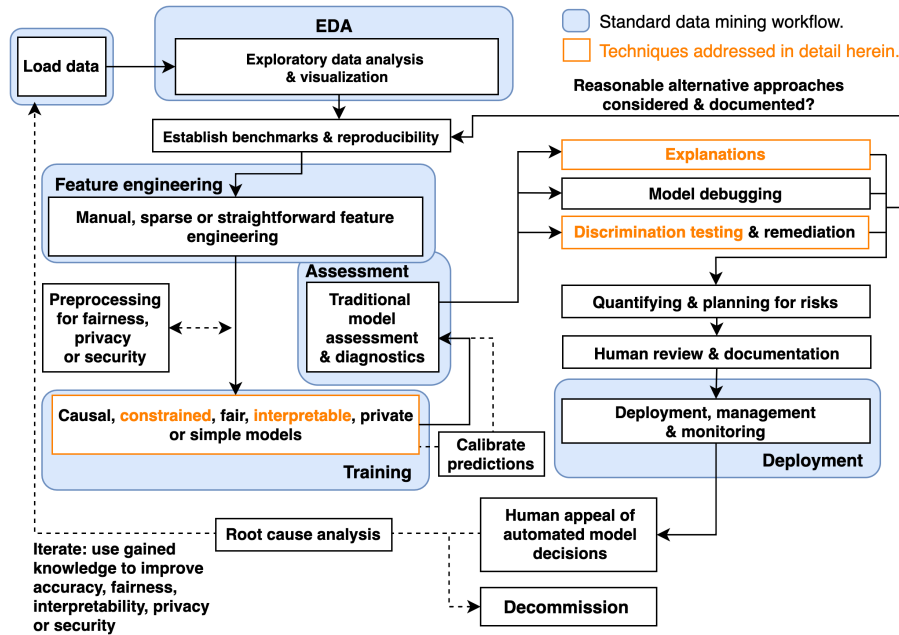


**Figure 8.** An example responsible ML workflow in which interpretable models, post-hoc explanations, discrimination testing and remediation techniques, among several other processes, can create an understandable and trustworthy ML system for high-stakes, human-centered, or regulated applications.

395 Any discussion of interpretable ML models would be incomplete without references to the  
 396 seminal work of the Rudin group at Duke University and EBMs, or GA<sup>2</sup>Ms, pioneered by researchers  
 397 at Microsoft and Cornell. In keeping with a major theme of this manuscript, models from these leading  
 398 researchers and several other kinds of interpretable ML models are now available as open source  
 399 Python packages. Among several types of currently available interpretable models, practitioners can  
 400 now use Python to evaluate EBM in the [interpret](#) package, optimal sparse decision trees, GAMs in  
 401 the [pyGAM](#) package, a variant of Friedman's RuleFit in the [skope-rules](#) package, monotonic calibrated  
 402 interpolated lookup tables in [tensorflow/lattice](#), and *this looks like that* interpretable deep learning  
 403 [33], [34], [35], [36].<sup>13,14</sup> Additional, relevant references and Python functionality include:

- 404 • **Exploratory data analysis (EDA):** H2OAggregatorEstimator in [h2o](#) [37].
- 405 • **Sparse feature extraction:** H2OGeneralizedLowRankEstimator in [h2o](#) [38].
- 406 • **Preprocessing & models for privacy:** [diffprivlib](#), [tensorflow/privacy](#) [39], [40], [41], [42].
- 407 • **Causal inference & probabilistic programming:** [dowhy](#), [PyMC3](#) [43].
- 408 • **Post-hoc explanation:** structured data explanations with [alibi](#) and [PDPbox](#), image classification  
 409 explanations with [DeepExplain](#), and natural language explanations with [allenlp](#) [44], [45], [46].
- 410 • **Discrimination testing:** [aequitas](#), [Themis](#).
- 411 • **Discrimination remediation:** Reweighting, adversarial de-biasing, learning fair representations,  
 412 and reject option classification with [AIF360](#) [47], [48], [49], [50].
- 413 • **Model debugging:** [foolbox](#), [SALib](#), [tensorflow/cleverhans](#), and  
 414 [tensorflow/model-analysis](#) [51], [52], [53], [54].
- 415 • **Model documentation:** models cards [55], e.g., [GPT-2 model card](#), [Object Detection model card](#).

416 See [Awesome Machine Learning Interpretability](#) for a longer, community-curated metalist of related  
 417 software packages and resources.

<sup>13</sup> See: [Optimal sparse decision trees](#).

<sup>14</sup> See: [This looks like that](#) interpretable deep learning.

418 3.2. *Appeal and Override of Automated Decisions*

419 Interpretable models and post-hoc explanations can play an important role in increasing  
420 transparency into model mechanisms and predictions. As seen in Section 2, interpretable models  
421 often enable users to enforce domain knowledge-based constraints on model behavior, to ensure that  
422 models obey reasonable expectations, and to gain data-derived insights into the modeled problem  
423 domain. Post-hoc explanations generally help describe and summarize mechanisms and decisions,  
424 potentially yielding an even clearer understanding of ML models. Together they can allow for human  
425 learning from ML, certain types of regulatory compliance, and crucially, human appeal or override  
426 of automated model decisions [31]. Interpretable models and post-hoc explanations are likely good  
427 candidates for ML uses cases under the FCRA, ECOA, GDPR and other regulations that may require  
428 explanations of model decisions, and they are already used in the financial services industry today for  
429 model validation and other purposes.<sup>15,16</sup> Writ large, transparency in ML also facilitates additional  
430 responsible AI processes such as model debugging, model documentation, and logical appeal and  
431 override processes, some of which may also be required by applicable regulations.<sup>17</sup> Among these,  
432 providing persons affected by a model with the opportunity to appeal ML-based decisions may deserve  
433 the most attention. ML models are often wrong<sup>18</sup> and appealing black-box decisions can be difficult.<sup>2</sup>  
434 For high-stakes, human-centered, or regulated applications that are trusted with mission- or life-critical  
435 decisions, the ability to logically appeal or override inevitable wrong decisions is not only a possible  
436 prerequisite for compliance, but also a failsafe procedure for those affected by ML decisions.

437 3.3. *Discrimination Testing and Remediation in Practice*

438 A significant body of research has emerged around exploring and fixing ML discrimination [57].  
439 Methods can be broadly placed into two groups: more traditional methods that mitigate discrimination  
440 by searching across possible algorithmic and feature specifications, and many approaches that have  
441 been developed in the last 5–7 years that alter the training algorithm, preprocess training data, or  
442 post-process predictions in order to diminish class-control correlations or dependencies. Whether  
443 these more recent methods are suitable for a particular use case depends on the legal environment  
444 where a model is deployed and on the use case itself. For comments on why some recent techniques  
445 could result in regulatory non-compliance in certain scenarios, see Appendix G.

446 Of the newer class of fairness enhancing interventions, within-algorithm discrimination mitigation  
447 techniques that do not use class information may be more likely to be acceptable in highly regulated  
448 settings today. These techniques often incorporate a loss function where more discriminatory paths  
449 or weights are penalized and only used by the model if improvements in fit overcome some penalty.  
450 (The relative level of fit-to-discrimination penalty is usually determined via hyperparameter.) Other  
451 mitigation strategies that only alter hyperparameters or algorithm choice are also likely to be acceptable.  
452 Traditional feature selection techniques (e.g., those used in linear models and decision trees) are also  
453 likely to continue to be accepted in regulatory environments. For further discussion of techniques that  
454 can mitigate DI in US financial services, see Schmidt and Stephens [58].

455 Regardless of the methodology chosen to minimize disparities, advances in computing have  
456 enhanced the ability to search for less discriminatory models. Prior to these advances, only a small  
457 number of alternative algorithms could be tested for lower levels of disparity without causing infeasible

15 See: *Deep Insights into Explainability and Interpretability of Machine Learning Algorithms and Applications to Risk Management*.

16 Unfortunately, many non-consistent explanation methods can result in drastically different global and local feature importance values across different models trained on the same data or even for refreshing a model with augmented training data [32]. Consistency and accuracy guarantees are perhaps a factor in the growing momentum behind Shapley values as a candidate technique for generating consumer-specific adverse action notices for explaining and appealing automated ML-based decisions in highly-regulated settings, such as credit lending [56].

17 E.g.: *US Federal Reserve Bank SR 11-7: Guidance on Model Risk Management*.

18 “All models are wrong, but some are useful.” – George Box, Statistician (1919 - 2013)

458 delays in model implementation. Now, large numbers of models can be quickly tested for lower  
459 discrimination and better predictive quality. An additional opportunity arises as a result of ML itself:  
460 the well-known Rashomon effect, or the multiplicity of good ML models for most datasets. It is now  
461 feasible to train more models, find more good models, and test more models for discrimination, and  
462 among all those tested models, there are likely to be some with high predictive performance and low  
463 discrimination.

#### 464 3.4. Intersectional and Non-static Risks in Machine Learning

465 The often black-box nature of ML, the perpetuation or exacerbation of discrimination by ML, or  
466 the privacy harms and security vulnerabilities inherent in ML are each serious and difficult problems on  
467 their own. However, evidence is mounting that these harms can also manifest as complex intersectional  
468 challenges, e.g., the *fairwashing* or *scaffolding* of biased models with ML explanations, the privacy harms  
469 of ML explanations, or the adversarial poisoning of ML models to become discriminatory [8], [18],  
470 [19].<sup>19,20,21</sup> Practitioners should of course consider the discussed interpretable modeling, post-hoc  
471 explanation, and discrimination testing approaches as at least partial remedies to the black-box and  
472 discrimination issues in ML. However, they should also consider that explanations can ease model  
473 stealing, data extraction, and membership inference attacks, and that explanations can mask ML  
474 discrimination. Additionally, high-stakes, human-centered, or regulated ML systems should generally  
475 be built and tested with robustness to adversarial attacks as a primary design consideration, and  
476 specifically to prevent ML models from being poisoned or otherwise altered to become discriminatory.  
477 Accuracy, discrimination, and security characteristics of a system can change over time as well. Simply  
478 testing for these problems at training time, as presented in Section 2, is not adequate for high-stakes,  
479 human-centered, or regulated ML systems. Accuracy, discrimination, and security should be monitored  
480 in real-time and over time, as long as a model is deployed.

### 481 4. Conclusion

482 This text puts forward results on simulated data to provide some validation of constrained ML  
483 models, post-hoc explanation techniques, and discrimination testing methods. These same modeling,  
484 explanation, and discrimination testing approaches are then applied to more realistic mortgage data  
485 to provide an example of a responsible ML workflow for high-stakes, human-centered, or regulated  
486 ML applications. The discussed methodologies are solid steps toward interpretability, explanation,  
487 and minimal discrimination for ML decisions, which should ultimately enable increased fairness  
488 and logical appeal processes for ML decision subjects. Of course, there is more to the responsible  
489 practice of ML than interpretable models, post-hoc explanation, and discrimination testing, even from  
490 a technology perspective, and Section 3 also points out numerous additional references and open  
491 source Python software assets that are available to researchers and practitioners today to increase  
492 human trust and understanding in ML systems. While the complex and messy problems of racism,  
493 sexism, privacy violations, and cyber crime can probably never be solved by technology alone, this  
494 work (and many others) illustrate numerous ways for ML practitioners to mitigate such risks.

495 **Author Contributions:** NG, data cleaning, GBM and MGBM assessment and results; PH, primary author; KM,  
496 ANN and XNN implementation, assessment, and results; NS, secondary author, data simulation and collection,  
497 and discrimination testing.

498 **Funding:** This work received no external funding.

<sup>19</sup> See: [Tay, Microsoft's AI chatbot, gets a crash course in racism from Twitter](#).

<sup>20</sup> While the focus of this paper is not ML security, proposed best-practices from that field do point to transparency of ML systems as a mitigating factor for some ML attacks and hacks [54]. High system complexity is sometimes considered a mitigating influence as well [59]. This is sometimes known as the *transparency paradox* in data privacy and security, and it likely applies to ML security as well, especially in the context of interpretable ML models and post-hoc explanation.

<sup>21</sup> See: [The AI Transparency Paradox](#).

**Acknowledgments:** Wen Phan for work in formalizing notation. Sue Shay for editing. Andrew Burt for ideas around the transparency paradox.

**Conflicts of Interest:** XNN was first made public by the corporate model validation team at Wells Fargo bank. Wells Fargo is a customer of, and investor in, H2O.ai and a client of BLDS, LLC. However, communications regarding XNN between Wells Fargo and the authors have been extremely limited prior to and during the drafting of this manuscript. Moreover, Wells Fargo exerted absolutely no editorial control over the text or results herein.

## Abbreviations

The following abbreviations are used in this text: AI – artificial intelligence, AIR - adverse impact ratio, ALE - accumulated local effect, ANN – artificial neural network, APR – annual percentage rate, AUC – area under the curve, CFPB – Consumer Financial Protection Bureau, DI – disparate impact, DT – disparate treatment, DTI – debt to income, EBM or GA<sup>2</sup>M – explainable boosting machine, i.e. variants GAMs that consider two-way interactions and may incorporate boosting into training, EEOC – Equal Employment Opportunity Commission, ECOA - Equal Credit Opportunity Act, EDA – exploratory data analysis, EU – European Union, FCRA – Fair Credit Reporting Act, FNR – false negative rate, FPR – false positive rate, GAM – generalized additive model, GBM – gradient boosting machine, GDPR - General Data Protection Regulation, HMDA – Home Mortgage Disclosure Act, ICE – individual conditional expectation, LTV – loan to value, MCC – Matthews correlation coefficient, ME – marginal effect, MGBM – monotonic gradient boosting machine, ML – machine learning, PD – partial dependence, RMSE – root mean square error, SGD – stochastic gradient descent, SHAP – SHapley Additive exPlanation, SMD - standardized mean difference, SR – supervision and regulation, US – United States, XNN – explainable neural network.

## Appendix A. Mortgage Data Details

The US HMDA law, originally enacted in 1975, requires many financial institutions that originate mortgage products to provide certain loan-level data about many types of mortgage-related products on an annual basis. This information is first provided to the CFPB, which subsequently releases some of the data to the public. Regulators often use HMDA data to, "...show whether lenders are serving the housing needs of their communities; they give public officials information that helps them make decisions and policies; and they shed light on lending patterns that could be discriminatory."<sup>5</sup> In addition to regulatory use, public advocacy groups use these data for similar purposes, and the lenders themselves use the data to benchmark their community outreach relative to their peers. The publicly available data that the CFPB releases includes information such as the lender, the type of loan, loan amount, LTV ratio, DTI ratio, and other important financial descriptors. The data also include information on each borrower and co-borrower's race, ethnicity, gender, and age. Because the data includes information on these protected class characteristics, certain measures that can be indicative of discrimination in lending can be calculated directly using the HDMA data. Ultimately, the HMDA data represent the most comprehensive source of data on highly-regulated mortgage lending that is publicly available, which makes it an ideal dataset to use for the types of analyses set forth in Sections 1 and 2.

## Appendix B. Selected Algorithmic Details

### Appendix B.1. Notation

To facilitate descriptions of data, modeling, and other post-hoc techniques, notation for input and output spaces, datasets, and models is defined.

#### Appendix B.1.1. Spaces

- Input features come from the set  $\mathcal{X}$  contained in a  $P$ -dimensional input space,  $\mathcal{X} \subset \mathbb{R}^P$ . An arbitrary, potentially unobserved, or future instance of  $\mathcal{X}$  is denoted  $\mathbf{x}, \mathbf{x} \in \mathcal{X}$ .
- Labels corresponding to instances of  $\mathcal{X}$  come from the set  $\mathcal{Y}$ .

- 544 • Learned output responses of models are contained in the set  $\hat{\mathcal{Y}}$ .

545 Appendix B.1.2. Data

- 546 • An input dataset  $\mathbf{X}$  is composed of observed instances of the set  $\mathcal{X}$  with a corresponding dataset  
547 of labels  $\mathbf{Y}$ , observed instances of the set  $\mathcal{Y}$ .  
548 • Each  $i$ -th observed instance of  $\mathbf{X}$  is denoted as  $\mathbf{x}^{(i)} = [x_0^{(i)}, x_1^{(i)}, \dots, x_{p-1}^{(i)}]$ , with corresponding  $i$ -th  
549 labels in  $\mathbf{Y}$ ,  $\mathbf{y}^{(i)}$ , and corresponding predictions in  $\hat{\mathbf{Y}}$ ,  $\hat{\mathbf{y}}^{(i)}$ .  
550 •  $\mathbf{X}$  and  $\mathbf{Y}$  consist of  $N$  tuples of observed instances:  $[(\mathbf{x}^{(0)}, \mathbf{y}^{(0)}), (\mathbf{x}^{(1)}, \mathbf{y}^{(1)}), \dots, (\mathbf{x}^{(N-1)}, \mathbf{y}^{(N-1)})]$ .  
551 • Each  $j$ -th input column vector of  $\mathbf{X}$  is denoted as  $X_j = [x_j^{(0)}, x_j^{(1)}, \dots, x_j^{(N-1)}]^T$ .

552 Appendix B.1.3. Models

- 553 • A type of ML model  $g$ , selected from a hypothesis set  $\mathcal{H}$ , is trained to represent an unknown  
554 signal-generating function  $f$  observed as  $\mathbf{X}$  with labels  $\mathbf{Y}$  using a training algorithm  $\mathcal{A}$ :  $\mathbf{X}, \mathbf{Y} \xrightarrow{\mathcal{A}} g$ ,  
555 such that  $g \approx f$ .  
556 •  $g$  generates learned output responses on the input dataset  $g(\mathbf{X}) = \hat{\mathbf{Y}}$ , and on the general input  
557 space  $g(\mathcal{X}) = \hat{\mathcal{Y}}$ .  
558 • A model to be explained or tested for discrimination is denoted as  $g$ .

559 Appendix B.2. Monotonic Gradient Boosting Machine Details

560 For some  $g^{\text{MGBM}}$  model (see Equation 2), monotonic splitting rules,  $\Theta_b^{\text{mono}}$ , are selected in a greedy,  
561 additive fashion by minimizing a regularized loss function,  $\mathcal{L}$ , that considers known target labels,  $\mathbf{y}$ ,  
562 the predictions of all subsequently trained trees in  $g^{\text{MGBM}}, g_{b-1}^{\text{MGBM}}(\mathbf{X})$ , and the  $b$ -th tree splits applied  
563 to some instance  $\mathbf{x}$ ,  $T_b(\mathbf{x}; \Theta_b^{\text{mono}})$ , in a numeric error function (e.g., squared error, Huber error),  $l$ , in  
564 addition to a regularization term that penalizes complexity in the  $b$ -th tree,  $\Omega(T_b)$ . For the  $b$ -th iteration  
565 over  $N$  instances,  $\mathcal{L}_b$ , can generally be defined as:

$$\mathcal{L}_b = \sum_{i=0}^{N-1} l(y^{(i)}, g_{b-1}^{\text{MGBM}}(\mathbf{x}^{(i)}), T_b(\mathbf{x}^{(i)}; \Theta_b^{\text{mono}})) + \Omega(T_b) \quad (\text{A1})$$

566 In addition to  $\mathcal{L}$ ,  $g^{\text{MGBM}}$  training is characterized by monotonic splitting rules and constraints on tree  
567 node weights. Each binary splitting rule in  $T_b$ ,  $\theta_{b,j,k} \in \Theta_b$ , is associated with a feature,  $X_j$ , is the  $k$ -th  
568 split associated with  $X_j$  in  $T_b$ , and results in left,  $L$ , and right,  $R$ , child nodes with a numeric weights,  
569  $\{w_{b,j,k,L}, w_{b,j,k,R}\}$ . For terminal nodes,  $\{w_{b,j,k,L}, w_{b,j,k,R}\}$  can be direct numeric components of some  
570  $g^{\text{MGBM}}$  prediction. For two values,  $x_j^\alpha$  and  $x_j^\beta$ , of some feature  $X_j$ , where  $x_j^\alpha \leq x_j^\beta$ ,  $g^{\text{MGBM}}$  is positive  
571 monotonic with respect to  $X_j$  if  $g^{\text{MGBM}}(x_j^\alpha) \leq g^{\text{MGBM}}(x_j^\beta) \forall \{x_j^\alpha \leq x_j^\beta\} \in X_j$ . The following rules and  
572 constraints ensure positive monotonicity in  $\Theta_b^{\text{mono}}$ :

- 573 1. For the first and highest split in  $T_b$  involving  $X_j$ , any  $\theta_{b,j,0}$  resulting in  $T(x_j; \theta_{b,j,0}) =$   
574  $\{w_{b,j,0,L}, w_{b,j,0,R}\}$  where  $w_{b,j,0,L} > w_{b,j,0,R}$ , is not considered.
- 575 2. For any subsequent left child node involving  $X_j$ , any  $\theta_{b,j,k \geq 1}$  resulting in  $T(x_j; \theta_{b,j,k \geq 1}) =$   
576  $\{w_{b,j,k \geq 1,L}, w_{b,j,k \geq 1,R}\}$  where  $w_{b,j,k \geq 1,L} > w_{b,j,k \geq 1,R}$ , is not considered.
- 577 3. Moreover, for any subsequent left child node involving  $X_j$ ,  $T(x_j; \theta_{b,j,k \geq 1}) = \{w_{b,j,k \geq 1,L}, w_{b,j,k \geq 1,R}\}$ ,  
578  $\{w_{b,j,k \geq 1,L}, w_{b,j,k \geq 1,R}\}$  are bound by the associated  $\theta_{b,j,k-1}$  set of node weights,  
579  $\{w_{b,j,k-1,L}, w_{b,j,k-1,R}\}$ , such that  $\{w_{b,j,k \geq 1,L}, w_{b,j,k \geq 1,R}\} < \frac{w_{b,j,k-1,L} + w_{b,j,k-1,R}}{2}$ .
- 580 4. (1) and (2) are also applied to all right child nodes, except that for right child nodes  $w_{b,j,k,L} \leq$   
581  $w_{b,j,k,R}$  and  $\{w_{b,j,k \geq 1,L}, w_{b,j,k \geq 1,R}\} \geq \frac{w_{b,j,k-1,L} + w_{b,j,k-1,R}}{2}$ .

582 Note that for any one  $X_j$  and subtree in  $g^{\text{MGBM}}$ , left subtrees will always produce lower predictions than  
583 right subtrees, and that any  $g^{\text{MGBM}}(\mathbf{x})$  is an addition of each full  $T_b$  prediction, with the application  
584 of a monotonic logit or softmax link function for classification problems. Moreover, each tree's root

node corresponds to some constant node weight that by definition obeys monotonicity constraints,  $T(x_j^\alpha; \theta_{b,0}) = T(x_j^\beta; \theta_{b,0}) = w_{b,0}$ . Together these additional splitting rules and node weight constraints ensure that  $g^{\text{MGBM}}(x_j^\alpha) \leq g^{\text{MGBM}}(x_j^\beta) \forall \{x_j^\alpha \leq x_j^\beta\} \in X_j$ . For a negative monotonic constraint, i.e.,  $g^{\text{MGBM}}(x_j^\alpha) \geq g^{\text{MGBM}}(x_j^\beta) \forall \{x_j^\alpha \leq x_j^\beta\} \in X_j$ , left and right splitting rules and node weight constraints are switched. Also consider that MGBM models with independent monotonicity constraints between some  $X_j$  and  $y$  likely restrict non-monotonic interactions between multiple  $X_j$ . Moreover, if monotonicity constraints are not applied to all  $X_j \in \mathbf{X}$ , any strong non-monotonic signal in training data associated with some important  $X_j$  maybe forced onto some other arbitrary unconstrained  $X_j$  under some  $g^{\text{MGBM}}$  models, compromising the end goal of interpretability.

**594 Appendix B.3. Explainable Neural Network Details**

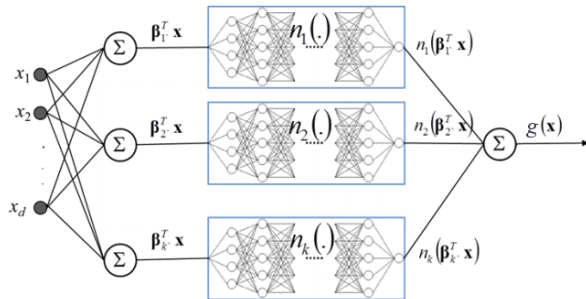


**Figure A1.** A general diagram of an XNN with three meta-layers: the bottom combination layer with  $K$  linear  $\sum_j \beta_{k,j} x_j$  hidden units, the middle metalayer with  $K$  hidden and separate  $n_k$  ridge functions, and the output combination layer that generates  $g^{\text{XNN}}(\mathbf{x})$  predictions. Figure adapted from Vaughan *et al.* [20].

**595**  $g^{\text{XNN}}$  is comprised of 3 meta-layers:

- 596** 1. The first and deepest meta-layer, composed of  $K$  linear  $\sum_j \beta_{k,j} x_j$  hidden units (see Equation 3), which should learn higher magnitude weights for each important input,  $X_j$ , is known as the *projection layer*. It is fully connected to each input  $X_j$ . Each hidden unit in the projection layer may optionally include a bias term.
- 600** 2. The second meta-layer contains  $K$  hidden and separate  $n_k$  ridge functions, or *subnetworks*. Each  $n_k$  is a neural network itself, which can be parameterized to suit a given modeling task. To facilitate direct interpretation and visualization, the input to each subnetwork is the 1-dimensional output of its associated projection layer  $\sum_j \beta_{k,j} x_j$  hidden unit. Each  $n_k$  can contain several bias terms.
- 604** 3. The output meta-layer, called the *combination layer*, is an output neuron comprised of a global bias term,  $\mu_0$ , and the  $K$  weighted 1-dimensional outputs of each subnetwork,  $\gamma_k n_k(\sum_j \beta_{k,j} x_j)$ . Again, each  $n_k$  subnetwork output into the combination layer is restricted to 1-dimension for interpretation and visualization purposes.

**608 Appendix B.4. One-dimensional Partial Dependence and Individual Conditional Expectation Details**

**609** Following Friedman *et al.* [13] a single input feature,  $X_j \in \mathbf{X}$ , and its complement set,  $\mathbf{X}_{\mathcal{P} \setminus \{j\}} \in \mathbf{X}$ , where  $X_j \cup \mathbf{X}_{\mathcal{P} \setminus \{j\}} = \mathbf{X}$  is considered.  $\text{PD}(X_j, g)$  for a given  $X_j$  is the estimated average output of the learned function  $g(\mathbf{x})$  when all the observed instances of  $X_j$  are set to a constant  $x^\gamma \in \mathcal{X}$  and  $\mathbf{X}_{\mathcal{P} \setminus \{j\}}$  is left unchanged.  $\text{ICE}(x_j, g)$  for a given instance  $\mathbf{x}$  and feature  $x_j$  is estimated as the output of  $g(\mathbf{x})$  when  $x_j$  is set to a constant  $x^\gamma \in \mathcal{X}$  and all other features  $\mathbf{x} \in \mathbf{X}_{\mathcal{P} \setminus \{j\}}$  are left untouched. PD and ICE curves are usually plotted over some set of constants drawn from  $\mathcal{X}$ , as displayed in Subsection 2.2.2 and Appendix E.1. Due to known problems for PD in the presence of strong correlation and interactions, PD should not be used alone. PD should be paired with ICE or be replaced with accumulated local effect (ALE) plots [22], [29].

618 *Appendix B.5. Shapley Value Details*

619 For some instance  $\mathbf{x} \in \mathcal{X}$ , Shapley explanations take the form:

$$g(\mathbf{x}) = \phi_0 + \sum_{j=0}^{|\mathcal{P}|-1} \phi_j z_j \quad (\text{A2})$$

620 In Equation A2,  $\mathbf{z} \in \{0,1\}^{\mathcal{P}}$  is a binary representation of  $\mathbf{x}$  where 0 indicates missingness. Each  
 621 Shapley value,  $\phi_j$ , is the local feature contribution value associated with  $x_j$ , and  $\phi_0$  is the average of  
 622  $g(\mathbf{X})$ . Each  $\phi_j$  is a weighted combination of model predictions with  $x_j$ ,  $g_x(S \cup \{j\})$ , and the model  
 623 predictions without  $x_j$ ,  $g_x(S)$ , for every possible subset of features  $S$  not including  $j$ ,  $S \subseteq \mathcal{P} \setminus \{j\}$ ,  
 624 where  $g_x$  incorporates the mapping between  $\mathbf{x}$  and the binary vector  $\mathbf{z}$ .

$$\phi_j = \sum_{S \subseteq \mathcal{P} \setminus \{j\}} \frac{|S|!(|\mathcal{P}| - |S| - 1)!}{\mathcal{P}!} [g_x(S \cup \{j\}) - g_x(S)] \quad (\text{A3})$$

625 Local, per-instance explanations using Shapley values tend to involve ranking  $x_j \in \mathbf{x}$  by  $\phi_j$  values or  
 626 delineating a set of the  $X_j$  names associated with the  $k$ -largest  $\phi_j$  values for some  $\mathbf{x}$ , where  $k$  is some  
 627 small positive integer, say 5. Global explanations are typically the absolute mean of the  $\phi_j$  associated  
 628 with a given  $X_j$  across all of the instances in some set  $\mathbf{X}$ .

629 **Appendix C. Types of Machine Learning Discrimination in US Legal and Regulatory Settings**

630 It is important to explain and draw a distinction between the two major types of discrimination  
 631 recognized in US legal and regulatory settings, disparate treatment (DT) and disparate impact (DI).  
 632 DT occurs most often in an algorithmic setting when a model explicitly uses protected class status  
 633 (e.g., race, sex) as an input feature or uses a feature that is so similar to protected class status that it  
 634 essentially proxies for class membership. With some limited exceptions, the use of these factors in an  
 635 algorithm is illegal under several statutes in the US.<sup>4</sup> DI occurs when some element of a decisioning  
 636 process includes a *facially neutral* factor (i.e., a reasonable and valid predictor of response) that results  
 637 in a disproportionate share of a protected class receiving an unfavorable outcome. In modeling, this is  
 638 most typically driven by a statistically important feature that is distributed unevenly across classes,  
 639 which causes more frequent unfavorable outcomes for the protected class. However, other factors,  
 640 such as hyperparameter or algorithm choices, can drive DI. Crucially, legality hinges on whether  
 641 changing the model, for example exchanging one feature for another or altering the hyperparameters  
 642 of an algorithm, can lead to a similarly predictive model with lower DI.

643 **Appendix D. Practical vs. Statistical Significance for Discrimination Testing**

644 A finding of *practical significance* means that discovered disparity is not only statistically significant,  
 645 but also passes beyond a chosen threshold that would constitute *prima facia* evidence of illegal  
 646 discrimination. Practical significance acknowledges that any large dataset is likely to show statistically  
 647 significant differences in outcomes by class, even if those differences are not truly meaningful. It further  
 648 recognizes that there are likely to be situations where differences in outcomes are beyond a model  
 649 user's ability to correct them without significantly degrading the quality of the model. Moreover,  
 650 practical significance is also needed by model builders and compliance personnel to determine whether  
 651 a model should undergo remediation efforts before it is put into production. Unfortunately, guidelines  
 652 for practical significance, i.e., the threshold at which any statistically significant disparity would  
 653 be considered evidence of illegal discrimination, are not as frequently codified as the standards for  
 654 statistical significance. One exception, however, is in employment discrimination analyses, where the  
 655 US Equal Employment Opportunity Commission (EEOC) has stated that if the AIR is below 0.80 and  
 656 statistically significant, then this constitutes *prima facia* evidence of discrimination, which the model

657 user must rebut in order for the DI not to be considered illegal discrimination.<sup>22</sup> It is important to  
 658 note that the 0.80 measure of practical significance, also known as the *80% rule* and the *4/5ths rule*, is  
 659 explicitly used in relation to AIR, and it is not clear that the use of this threshold is directly relevant to  
 660 testing fairness for measures other than the AIR.

661 The legal thresholds for determining statistical significance is clearer and more consistent than that  
 662 for practical significance. The first guidance in US courts occurred in a case involving discrimination  
 663 in jury selection, *Castaneda vs. Partida*.<sup>23</sup> Here, the US Supreme Court wrote that, “As a general rule for  
 664 such large samples, if the difference between the expected value and the observed number is greater  
 665 than two or three standard deviations, then the hypothesis that the jury drawing was random would  
 666 be suspect to a social scientist.” This “two or three standard deviations” test was then applied to  
 667 employment discrimination in *Hazelwood School Districts vs. United States*.<sup>24</sup> Out of this, a 5% two-sided  
 668 test ( $z=1.96$ ), or an equivalent 2.5% one-sided test, has become a common standard for determining  
 669 whether evidence of disparities is statistically significant.

## 670 Appendix E. Additional Simulated Data Results

671 As seen in Subsection 2.1.1, little or no trade-off is required in terms of model to fit to use the  
 672 constrained models. Hence, intrinsic interpretability, post-hoc explainability, and discrimination are  
 673 explored further for the  $g^{\text{MGBM}}$  and  $g^{\text{XNN}}$  models in Appendices E.1 - E.2. Intrinsic interpretability  
 674 for  $g^{\text{MGBM}}$  is evaluated with PD and ICE, and post-hoc explainability is highlighted via global and  
 675 local Shapley explanations. For  $g^{\text{XNN}}$ , Shapley explanation techniques are also used to generate global  
 676 and local feature importance to augment interpretability results exhibited in Subection 2.1.2. Both  
 677  $g^{\text{MGBM}}(\mathbf{X})$  and  $g^{\text{XNN}}(\mathbf{X})$  are evaluated for discrimination using AIR, ME, SMD, and other measures.

### 678 Appendix E.1. Interpretability and Post-hoc Explanation Results

679 Global mean absolute Shapley value feature importance for  $g^{\text{MGBM}}(\mathbf{X})$  on the simulated test data  
 680 is displayed in Figure A2.

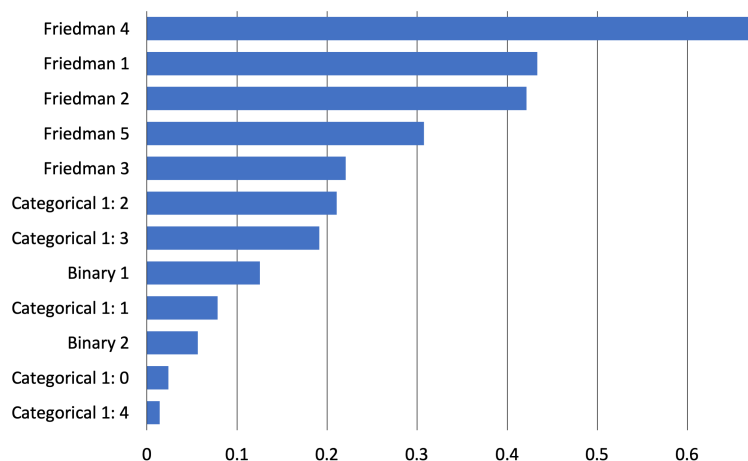


Figure A2. Global mean absolute Tree SHAP feature importance for  $g^{\text{MGBM}}(\mathbf{X})$  on the simulated test data.

<sup>22</sup> Importantly, the standard of 0.80 is not a law, but a rule of thumb for agencies tasked with enforcement of discrimination laws. “Adoption of Questions and Answers To Clarify and Provide a Common Interpretation of the Uniform Guidelines on Employee Selection Procedures,” Federal Register, Volume 44, Number 43 (1979).

<sup>23</sup> *Castaneda vs. Partida*, 430 US 482 - Supreme Court (1977)

<sup>24</sup> *Hazelwood School Dist. vs. United States*, 433 US 299 (1977)

As expected, the  $X_{Friedman,j}$  features from the original Friedman [10] and Friedman *et al.* [11] formula are the main drivers of  $g^{\text{MGBM}}(\mathbf{X})$  predictions, with encoded versions of the augmented categorical and binary features contributing less on average to  $g^{\text{MGBM}}(\mathbf{X})$  predictions.

Figure A3 highlights PD, ICE, and histograms of the most important features from Figure A2.

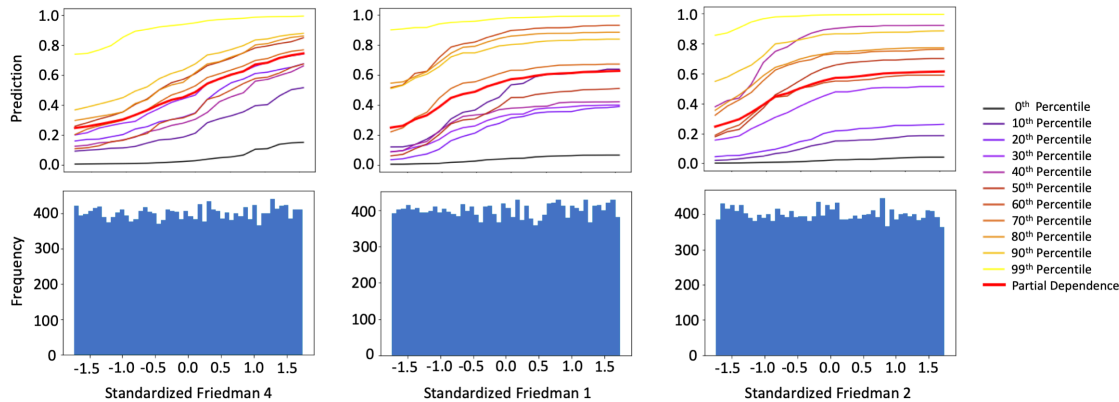


**Figure A3.** PD, ICE for 10 instances across selected percentiles of  $g^{\text{MGBM}}(\mathbf{X})$ , and histograms for the three most important input features of  $g^{\text{MGBM}}$  on the simulated test data.

$X_{Friedman,1}$ ,  $X_{Friedman,2}$ , and  $X_{Friedman,4}$  were positively monotonically constrained under  $g^{\text{MGBM}}$  for the simulated data, and positive monotonicity looks to be confirmed on average with PD and at numerous local percentiles of  $g^{\text{MGBM}}(\mathbf{X})$  with ICE. As the PD curves generally follow the patterns of the ICE curves, PD is likely an accurate representation of average feature behavior for  $X_{Friedman,1}$ ,  $X_{Friedman,2}$ , and  $X_{Friedman,4}$ . Also because PD and ICE curves do not obviously diverge,  $g^{\text{MGBM}}$  is likely not modeling strong interactions, despite the fact that known interactions are included in the simulated data signal-generating function in Equation 1. The one-dimensional monotonic constraints may hinder the modeling of non-monotonic interactions, but do not strongly affect overall  $g^{\text{MGBM}}$  accuracy, perhaps due to the main drivers,  $X_{Friedman,1}$ ,  $X_{Friedman,2}$ , and  $X_{Friedman,4}$ , all being constrained in the same direction and able to weakly interact as needed.

Local Shapley values for records at the 10<sup>th</sup>, 50<sup>th</sup>, and 90<sup>th</sup> percentiles of  $g^{\text{MGBM}}(\mathbf{X})$  in the simulated test data are displayed in Figure A4.

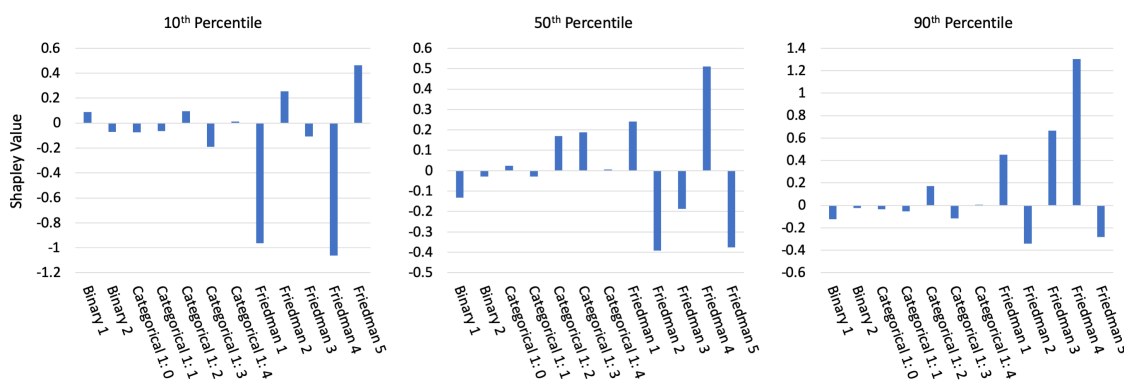


**Figure A4.** Tree SHAP values for three instances across selected percentiles of  $g^{\text{MGBM}}(\mathbf{X})$  for the simulated test data.

The Shapley values in Figure A4 appear to be a logical result. For the lower prediction at the 10<sup>th</sup> percentile of  $g^{\text{MGBM}}(\mathbf{X})$ , the largest local contributions are negative and the majority of local contributions are also negative. At the median of  $g^{\text{MGBM}}(\mathbf{X})$ , local contributions are roughly split between positive and negative values, and at the 90<sup>th</sup> of  $g^{\text{MGBM}}(\mathbf{X})$ , most large contributions are

positive. In each case, large local contributions generally follow global importance results in Figure A2 as well.

Figure A5 shows global mean absolute Shapley feature importance for  $g^{XNN}(\mathbf{X})$  on the simulated test data, using the approximate Deep SHAP technique.

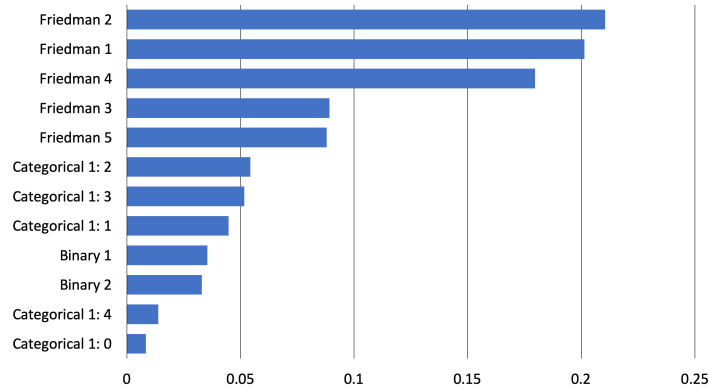


**Figure A5.** Global mean Deep SHAP feature importance for  $g^{XNN}(\mathbf{X})$  on the simulated test data.

Like  $g^{MGBM}$ ,  $g^{XNN}$  ranks the  $X_{Friedman,j}$  features higher in terms of importance than the categorical and binary features. The consistency between the feature rankings of  $g^{MGBM}$  and  $g^{XNN}$  is somewhat striking, given their different hypothesis families and architectures. Both  $g^{MGBM}$  and  $g^{XNN}$  rank  $X_{Friedman,1}$ ,  $X_{Friedman,2}$ , and  $X_{Friedman,4}$  as the most important features, both place  $X_{Categorical,2}$  and  $X_{Categorical,3}$  above the  $X_{Binary,1}$  and  $X_{Binary,2}$  features, both rank  $X_{Binary,1}$  above  $X_{Binary,2}$ , and both place the least importance on  $X_{Categorical,4}$  and  $X_{Categorical,0}$ .

Local Deep SHAP feature importance in Figure A6 supplements the global interpretability of  $g^{XNN}$  displayed in Figures A5 and 1. Local Deep SHAP values are extracted from the projection layer of  $g^{XNN}$  and reported in the probability space. Deep SHAP values can be calculated for any arbitrary  $g^{XNN}(\mathbf{x})$ , allowing for detailed, local summarization of individual model predictions.

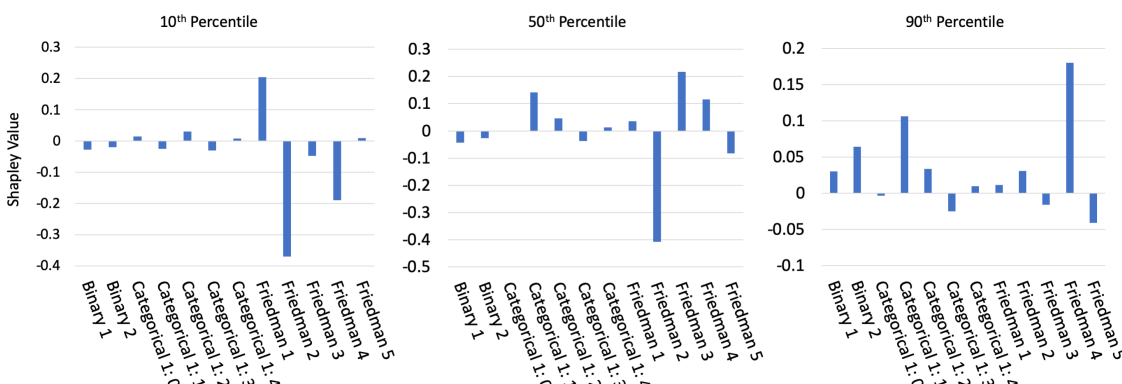


**Figure A6.** Deep SHAP values for three instances across selected percentiles of  $g^{XNN}(\mathbf{X})$  on the simulated test data.

As expected, Deep SHAP values generally increase from the 10<sup>th</sup> percentile of  $g^{XNN}(\mathbf{X})$  to the 90<sup>th</sup> percentile of  $g^{XNN}(\mathbf{X})$ , with primarily important global drivers of model behavior contributing to the selected local  $g^{XNN}(\mathbf{x})$  predictions.

#### 718 Appendix E.2. Discrimination Testing Results

Tables A1a and A1b show the results of the disparity tests using the simulated data for two hypothetical sets of class-control groups. Several measures of disparities are shown, with the SMDs calculated using the probabilities from  $g^{MGBM}(\mathbf{X})$  and  $g^{XNN}(\mathbf{X})$ , FNRs, their ratios, MEs, and AIRs

calculated using a binary outcome based on a cutoff of 0.6 (anyone with probabilities of 0.6 or greater receives the favorable outcome).<sup>11</sup>

Since  $g^{\text{MGBM}}$  and  $g^{\text{XNN}}$  assume that a higher score is favorable (as might be the case if the model were predicting responses to marketing offers), one might consider the relative FNRs as a measure of the class-control disparities. Table A1b shows that protected group 1 has higher relative FNRs under  $g^{\text{XNN}}$  (1.13 vs. 1.06). However, in Table A1a the overall FNRs were lower for  $g^{\text{XNN}}$  (0.357 vs. 0.401). This illustrates a danger in considering relative class-control measures in isolation when comparing across models: despite the  $g^{\text{MGBM}}$  appearing to be a relatively fairer model, more protected group 1 members experience negative outcomes using  $g^{\text{MGBM}}$ . This is because FNR accuracy improves for both the protected group 1 and control group 1, but members of control group 1 benefit more than those in protected group 1. Of course, the choice of which model is truly fairer is a policy question.

(a) Group size, accuracy, and FNR for  $g^{\text{MGBM}}(\mathbf{X})$  and  $g^{\text{XNN}}(\mathbf{X})$  on the simulated test data.

Class	N	Model	Accuracy↑	FNR↓
Protected 1	3,057	$g^{\text{MGBM}}$	0.770	0.401
		$g^{\text{XNN}}$	0.771	0.357
Control 1	16,943	$g^{\text{MGBM}}$	0.739	0.378
		$g^{\text{XNN}}$	0.756	0.314
Protected 2	9,916	$g^{\text{MGBM}}$	0.758	0.331
		$g^{\text{XNN}}$	0.762	0.302
Control 2	10,084	$g^{\text{MGBM}}$	0.729	0.420
		$g^{\text{XNN}}$	0.756	0.332

(b) AIR, ME, SMD, and FNR ratio for  $g^{\text{MGBM}}(\mathbf{X})$  and  $g^{\text{XNN}}(\mathbf{X})$  on the simulated test data.

Model	Protected Class	Control Class	AIR↑	ME↓	SMD↓	FNR Ratio↓
$g^{\text{MGBM}}$	1	1	0.752	9.7%	-0.206	1.06
	2	2	1.10	-3.6%	0.106	0.788
$g^{\text{XNN}}$	1	1	0.727	12.0%	-0.274	1.13
	2	2	0.976	1.0%	0.001	0.907

**Table A1.** Discrimination measures for the simulated test data. Arrows indicate the direction of improvement for each measure.

For  $g^{\text{XNN}}(\mathbf{X})$ , 12.0% fewer control group 1 members receive the favorable offer under the ME column in Table A1b. Of note is that 12.0% is not a meaningful difference without context. If the population of control group 1 and control group 2 were substantially similar in relevant characteristics, 12.0% could represent an extremely large difference and would require remediation. But if they represent substantially different populations, then 12.0% could represent a reasonable deviation from parity. As an example, if a lending institution that has traditionally focused on high credit quality clients were to expand into previously under-banked communities, an 12.0% class-control difference in loan approval rates might be expected because the average credit quality of the new population would be lower than that of the existing population. Protected group 1's AIR under  $g^{\text{XNN}}$  is 0.727, below the EEOC 4/5ths rule threshold. It is also highly statistically significant (not shown, but available in resources discussed in Subsection 1.8). Together these would indicate that there may be evidence of illegal DI. As with ME and other measures, the reasonableness of this disparity is not clear outside of context. However, most regulated institutions that do perform discrimination analyses would find an AIR of this magnitude concerning and warranting further review. Some pertinent remediation strategies for discovered discrimination are discussed in Subsection 3.3.

SMD is used here to measure  $g^{\text{MGBM}}(\mathbf{X})$  and  $g^{\text{XNN}}(\mathbf{X})$  probabilities prior to being transformed into classifications. (This measurement would be particularly relevant if the probabilities are used in combination with other models to determine an outcome.) The results show that  $g^{\text{MGBM}}(\mathbf{X})$  has less DI than  $g^{\text{XNN}}(\mathbf{X})$  (-0.206 vs. -0.274), but both are close to Cohen's small effect threshold of -0.20. Whether a small effect would be a highlighted concern would depend on a organization's chosen threshold for flagging models for further review.

**754 Appendix F. Discrimination Testing and Cutoff Selection**

755 The selection of which cutoff to use in production is typically based on the model's use case, rather  
756 than one based solely on the statistical properties of the predictions themselves. For example, a model  
757 developer at a bank might build a credit model where the F1 score is maximized at a delinquency  
758 probability cutoff of 0.15. For purposes of evaluating the quality of the model, she may review  
759 confusion matrix statistics (accuracy, recall, precision, etc.) using cutoffs based on the maximum F1  
760 score. But, because of its risk tolerance and other factors, the bank itself might be willing to lend to  
761 anyone with a delinquency probability of 0.18 or lower, which would mean that anyone who is scored  
762 at 0.18 or lower would receive an offer of credit. Because disparity analyses are concerned with how  
763 people are affected by the deployed model, it is essential that any confusion matrix-based measures of  
764 disparity be calculated on the in-production classification decisions, rather than on cutoffs that are not  
765 related to what those affected by the model will experience.

**766 Appendix G. Recent Fairness Techniques in US Legal and Regulatory Settings**

767 Great care must be taken to ensure that the appropriate discrimination measures are employed  
768 for any given use case. Additionally, the effects of changing a model must be viewed holistically.  
769 For example, the mortgage data disparity analysis in Subsection 2.2.3 shows that if one were to  
770 choose  $g^{\text{MGBM}}$  over  $g^{\text{XNN}}$  because  $g^{\text{MGBM}}$  has a lower FPR ratio for blacks, it would ultimately lead  
771 to a higher FPR for blacks overall, which may represent doing more harm than good. Furthermore,  
772 using some recently developed discrimination mitigation methods may lead to non-compliance with  
773 anti-discrimination laws and regulations. A fundamental maxim of US anti-discrimination law is that  
774 (to slightly paraphrase), "similarly situated people should be treated similarly."<sup>25</sup> A model developed  
775 without inclusion of class status (or proxies thereof) considers similarly situated people the same on the  
776 dimensions included in the model: people who have the same feature values will have the same model  
777 output (though there may be some small or random differences in outcomes due to computational  
778 issues). Obviously, the inclusion of protected class status will change model output by class. With  
779 possible rare exceptions, this is likely to be viewed with legal and regulatory skepticism today, even if  
780 including class status is done with fairness as the goal.<sup>26</sup> Preprocessing and post-processing techniques  
781 may be similarly problematic, because industries that must provide explanations to those who receive  
782 unfavorable treatment (e.g., adverse action notices in US financial services) may have to incorporate  
783 the class adjustments into their explanations as well.

**784 References**

- 785 1. Rudin, C. Please Stop Explaining Black Box Models for High Stakes Decisions and Use Interpretable  
786 Models Instead. *arXiv preprint arXiv:1811.10154* **2018**. URL: <https://arxiv.org/pdf/1811.10154.pdf>.
- 787 2. Feldman, M.; Friedler, S.A.; Moeller, J.; Scheidegger, C.; Venkatasubramanian, S. Certifying and Removing  
788 Disparate Impact. Proceedings of the 21<sup>st</sup> ACM SIGKDD International Conference on Knowledge  
789 Discovery and Data Mining. ACM, 2015, pp. 259–268. URL: <https://arxiv.org/pdf/1412.3756.pdf>.
- 790 3. Dwork, C.; Hardt, M.; Pitassi, T.; Reingold, O.; Zemel, R. Fairness Through Awareness. Proceedings  
791 of the 3rd Innovations in Theoretical Computer Science Conference. ACM, 2012, pp. 214–226. URL:  
792 <https://arxiv.org/pdf/1104.3913.pdf>.

25 In the pay discrimination case, *Bazemore vs. Friday*, 478 US 385 (1986), the US Supreme Court found that, "Each week's paycheck that delivers less to a black than to a similarly situated white is a wrong actionable ..." Beyond the obvious conceptual meaning, what specifically constitutes *similarly situated* is controversial and its interpretation differs by circuit.

26 In a reverse discrimination case, *Ricci v Desafano*, 557 US 557 (2009), the court found that any consideration of race which is not justified by correcting for past proven discrimination is illegal and, moreover, a lack of fairness is not necessarily evidence of illegal discrimination.

- 793 4. Buolamwini, J.; Gebru, T. Gender Shades: Intersectional Accuracy Disparities in Commercial Gender  
794 Classification. Conference on Fairness, Accountability and Transparency, 2018, pp. 77–91. URL: <http://proceedings.mlr.press/v81/buolamwini18a/buolamwini18a.pdf>.
- 795 5. Barreno, M.; Nelson, B.; Joseph, A.D.; Tygar, J. The Security of Machine Learning. *Machine Learning* **2010**,  
796 *81*, 121–148. URL: [http://people.ischool.berkeley.edu/~tygar/papers/SML/sec\\_mach\\_learn\\_journal.pdf](http://people.ischool.berkeley.edu/~tygar/papers/SML/sec_mach_learn_journal.pdf).
- 797 6. Tramèr, F.; Zhang, F.; Juels, A.; Reiter, M.K.; Ristenpart, T. Stealing Machine Learning Models via  
798 Prediction APIs. 25th {USENIX} Security Symposium ({USENIX} Security 16), 2016, pp. 601–618. URL:  
799 [https://www.usenix.org/system/files/conference/usenixsecurity16/sec16\\_paper\\_tramer.pdf](https://www.usenix.org/system/files/conference/usenixsecurity16/sec16_paper_tramer.pdf).
- 800 7. Shokri, R.; Stronati, M.; Song, C.; Shmatikov, V. Membership Inference Attacks Against Machine Learning  
801 Models. 2017 IEEE Symposium on Security and Privacy (SP). IEEE, 2017, pp. 3–18. URL: <https://arxiv.org/pdf/1610.05820.pdf>.
- 802 8. Shokri, R.; Strobel, M.; Zick, Y. Privacy Risks of Explaining Machine Learning Models. *arXiv preprint*  
803 *arXiv:1907.00164* **2019**. URL: <https://arxiv.org/pdf/1907.00164.pdf>.
- 804 9. Williams, M.; others. *Interpretability*; Fast Forward Labs, 2017. URL: <https://www.cloudera.com/products/fast-forward-labs-research.html>.
- 805 10. Friedman, J.H. A Tree-structured Approach to Nonparametric Multiple Regression. In *Smoothing Techniques*  
806 for Curve Estimation; Springer, 1979; pp. 5–22. URL: <http://inspirehep.net/record/140963/files/slac-pub-2336.pdf>.
- 807 11. Friedman, J.H.; others. Multivariate Adaptive Regression Splines. *The Annals of Statistics* **1991**, *19*, 1–67.  
808 URL: [https://projecteuclid.org/download/pdf\\_1/euclid-aos/1176347963](https://projecteuclid.org/download/pdf_1/euclid-aos/1176347963).
- 809 12. Friedman, J.H. Greedy Function Approximation: a Gradient Boosting Machine. *The Annals of Statistics*  
810 **2001**, pp. 1189–1232. URL: [https://projecteuclid.org/download/pdf\\_1/euclid-aos/1013203451](https://projecteuclid.org/download/pdf_1/euclid-aos/1013203451).
- 811 13. Friedman, J.H.; Hastie, T.; Tibshirani, R. *The Elements of Statistical Learning*; Springer: New York, 2001.  
812 URL: [https://web.stanford.edu/~hastie/ElemStatLearn/printings/ESLII\\_print12.pdf](https://web.stanford.edu/~hastie/ElemStatLearn/printings/ESLII_print12.pdf).
- 813 14. Recht, B.; Re, C.; Wright, S.; Niu, F. HOGWILD: A Lock-free Approach to Parallelizing  
814 Stochastic Gradient Descent. Advances in Neural Information Processing Systems (NIPS), 2011,  
815 pp. 693–701. URL: <https://papers.nips.cc/paper/4390-hogwild-a-lock-free-approach-to-parallelizing-stochastic-gradient-descent.pdf>.
- 816 15. Hinton, G.E.; Srivastava, N.; Krizhevsky, A.; Sutskever, I.; Salakhutdinov, R.R. Improving Neural Networks  
817 by Preventing Co-adaptation of Feature Detectors. *arXiv preprint arXiv:1207.0580* **2012**. URL: <https://arxiv.org/pdf/1207.0580.pdf>.
- 818 16. Sutskever, I.; Martens, J.; Dahl, G.; Hinton, G. On the Importance of Initialization and Momentum  
819 in Deep Learning. International Conference on Machine Learning, 2013, pp. 1139–1147. URL: <http://proceedings.mlr.press/v28/sutskever13.pdf>.
- 820 17. Zeiler, M.D. ADADELTA: An Adaptive Learning Rate Method. *arXiv preprint arXiv:1212.5701* **2012**. URL:  
821 <https://arxiv.org/pdf/1212.5701.pdf>.
- 822 18. Aïvodji, U.; Arai, H.; Fortineau, O.; Gambs, S.; Hara, S.; Tapp, A. Fairwashing: The Risk of Rationalization.  
823 *arXiv preprint arXiv:1901.09749* **2019**. URL: <https://arxiv.org/pdf/1901.09749.pdf>.
- 824 19. Slack, D.; Hilgard, S.; Jia, E.; Singh, S.; Lakkaraju, H. Fooling LIME and SHAP: Adversarial Attacks on  
825 Post-hoc Explanation Methods. *arXiv preprint arXiv:1911.02508* **2019**. URL: <https://arxiv.org/pdf/1911.02508.pdf>.
- 826 20. Vaughan, J.; Sudjianto, A.; Brahimi, E.; Chen, J.; Nair, V.N. Explainable Neural Networks Based on Additive  
827 Index Models. *arXiv preprint arXiv:1806.01933* **2018**. URL: <https://arxiv.org/pdf/1806.01933.pdf>.
- 828 21. Yang, Z.; Zhang, A.; Sudjianto, A. Enhancing Explainability of Neural Networks Through Architecture  
829 Constraints. *arXiv preprint arXiv:1901.03838* **2019**. URL: <https://arxiv.org/pdf/1901.03838.pdf>.
- 830 22. Goldstein, A.; Kapelner, A.; Bleich, J.; Pitkin, E. Peeking Inside the Black Box: Visualizing Statistical  
831 Learning with Plots of Individual Conditional Expectation. *Journal of Computational and Graphical Statistics*  
832 **2015**, *24*. URL: <https://arxiv.org/pdf/1309.6392.pdf>.
- 833 23. Lundberg, S.M.; Lee, S.I. A Unified Approach to Interpreting Model Predictions. In *Advances in Neural*  
834 *Information Processing Systems (NIPS)*; Guyon, I.; Luxburg, U.V.; Bengio, S.; Wallach, H.; Fergus, R.;  
835 Vishwanathan, S.; Garnett, R., Eds.; Curran Associates, Inc., 2017; pp. 4765–4774. URL: <http://papers.nips.cc/paper/7062-a-unified-approach-to-interpreting-model-predictions.pdf>.

- 845 24. Lundberg, S.M.; Erion, G.G.; Lee, S.I. Consistent Individualized Feature Attribution for Tree Ensembles.  
846 In *Proceedings of the 2017 ICML Workshop on Human Interpretability in Machine Learning (WHI 2017)*; Kim,  
847 B.; Malioutov, D.M.; Varshney, K.R.; Weller, A., Eds.; ICML WHI 2017, 2017; pp. 15–21. URL: <https://openreview.net/pdf?id=ByTKSo-m->.
- 849 25. Cohen, J. *Statistical Power Analysis for the Behavioral Sciences*; Lawrence Erlbaum Associates, 1988.  
850 URL: <http://www.utstat.toronto.edu/~brunner/oldclass/378f16/readings/CohenPower.pdf>.
- 851 26. Cohen, J. A Power Primer. *Psychological Bulletin* **1992**, *112*, 155. URL: <https://www.ime.usp.br/~abe/lista/pdfn45sGokvRe.pdf>.
- 853 27. Zafar, M.B.; Valera, I.; Gomez Rodriguez, M.; Gummadi, K.P. Fairness Beyond Disparate Treatment &  
854 Disparate Impact: Learning Classification Without Disparate Mistreatment. Proceedings of the 26th  
855 International Conference on World Wide Web. International World Wide Web Conferences Steering  
856 Committee, 2017, pp. 1171–1180. URL: <https://arxiv.org/pdf/1610.08452.pdf>.
- 857 28. Lou, Y.; Caruana, R.; Gehrke, J.; Hooker, G. Accurate Intelligible Models with Pairwise Interactions.  
858 Proceedings of the 19th ACM SIGKDD International Conference on Knowledge Discovery and Data  
859 Mining. ACM, 2013, pp. 623–631. URL: <http://citeseerx.ist.psu.edu/viewdoc/download?doi=10.1.1.352.7682&rep=rep1&type=pdf>.
- 861 29. Apley, D.W. Visualizing the Effects of Predictor Variables in Black Box Supervised Learning Models. *arXiv preprint arXiv:1612.08468* **2016**. URL: <https://arxiv.org/pdf/1612.08468.pdf>.
- 863 30. Shapley, L.S.; Roth, A.E.; others. *The Shapley value: Essays in Honor of Lloyd S. Shapley*; Cambridge  
864 University Press, 1988. URL: <http://www.library.fa.ru/files/Roth2.pdf>.
- 865 31. Hall, P. On the Art and Science of Machine Learning Explanations. KDD '19 XAI Workshop, 2019. URL:  
866 <https://arxiv.org/pdf/1810.02909.pdf>.
- 867 32. Molnar, C. *Interpretable Machine Learning*; christophm.github.io, 2018. URL: <https://christophm.github.io/interpretable-ml-book/>.
- 869 33. Hu, X.; Rudin, C.; Seltzer, M. Optimal Sparse Decision Trees. *arXiv preprint arXiv:1904.12847* **2019**. URL:  
870 <https://arxiv.org/pdf/1904.12847.pdf>.
- 871 34. Friedman, J.H.; Popescu, B.E.; others. Predictive Learning Via Rule Ensembles. *The Annals of Applied  
872 Statistics* **2008**, *2*, 916–954. URL: [https://projecteuclid.org/download/pdfview\\_1/euclid.aoas/1223908046](https://projecteuclid.org/download/pdfview_1/euclid.aoas/1223908046).
- 873 35. Gupta, M.; Cotter, A.; Pfeifer, J.; Voevodski, K.; Canini, K.; Mangylov, A.; Moczydlowski, W.; Van Esbroeck,  
874 A. Monotonic Calibrated Interpolated Lookup Tables. *The Journal of Machine Learning Research* **2016**,  
875 *17*, 3790–3836. URL: <http://www.jmlr.org/papers/volume17/15-243/15-243.pdf>.
- 876 36. Chen, C.; Li, O.; Barnett, A.; Su, J.; Rudin, C. This Looks Like That: Deep Learning for Interpretable  
877 Image Recognition. Proceedings of Neural Information Processing Systems (NeurIPS), 2019. URL:  
878 <https://arxiv.org/pdf/1806.10574.pdf>.
- 879 37. Wilkinson, L. Visualizing Big Data Outliers through Distributed Aggregation. *IEEE Transactions on  
880 Visualization & Computer Graphics* **2018**. URL: <https://www.cs.uic.edu/~wilkinson/Publications/outliers.pdf>.
- 882 38. Udell, M.; Horn, C.; Zadeh, R.; Boyd, S.; others. Generalized Low Rank Models. *Foundations and Trends®  
883 in Machine Learning* **2016**, *9*, 1–118. URL: <https://www.nowpublishers.com/article/Details/MAL-055>.
- 884 39. Holohan, N.; Braghin, S.; Mac Aonghusa, P.; Levacher, K. Diffprivlib: The IBM Differential Privacy Library.  
885 *arXiv preprint arXiv:1907.02444* **2019**. URL: <https://arxiv.org/pdf/1907.02444.pdf>.
- 886 40. Ji, Z.; Lipton, Z.C.; Elkan, C. Differential Privacy and Machine Learning: A Survey and Review. *arXiv preprint arXiv:1412.7584* **2014**. URL: <https://arxiv.org/pdf/1412.7584.pdf>.
- 888 41. Papernot, N.; Song, S.; Mironov, I.; Raghunathan, A.; Talwar, K.; Erlingsson, Ú. Scalable Private Learning  
889 with PATE. *arXiv preprint arXiv:1802.08908* **2018**. URL: <https://arxiv.org/pdf/1802.08908.pdf>.
- 890 42. Abadi, M.; Chu, A.; Goodfellow, I.; McMahan, H.B.; Mironov, I.; Talwar, K.; Zhang, L. Deep Learning with  
891 Differential Privacy. Proceedings of the 2016 ACM SIGSAC Conference on Computer and Communications  
892 Security. ACM, 2016, pp. 308–318. URL: <https://arxiv.org/pdf/1607.00133.pdf>.
- 893 43. Pearl, J.; Mackenzie, D. *The Book of Why: The New Science of Cause and Effect*; Basic Books, 2018. URL: <http://cdar.berkeley.edu/wp-content/uploads/2017/04/Lisa-Goldberg-reviews-The-Book-of-Why.pdf>.
- 894 44. Wachter, S.; Mittelstadt, B.; Russell, C. Counterfactual Explanations without Opening the Black Box:  
895 Automated Decisions and the GDPR. *Harv. JL & Tech.* **2017**, *31*, 841. URL: <https://arxiv.org/pdf/1711.00399.pdf>.

- 898 45. Ancona, M.; Ceolini, E.; Oztireli, C.; Gross, M. Towards Better Understanding of Gradient-based Attribution  
899 Methods for Deep Neural Networks. 6th International Conference on Learning Representations (ICLR  
900 2018), 2018. URL: [https://www.research-collection.ethz.ch/bitstream/handle/20.500.11850/249929/Flow\\_ICLR\\_2018.pdf](https://www.research-collection.ethz.ch/bitstream/handle/20.500.11850/249929/Flow_ICLR_2018.pdf).
- 902 46. Wallace, E.; Tuyls, J.; Wang, J.; Subramanian, S.; Gardner, M.; Singh, S. AllenNLP Interpret: A Framework  
903 for Explaining Predictions of NLP Models. *arXiv preprint arXiv:1909.09251* **2019**. URL: <https://arxiv.org/pdf/1909.09251.pdf>.
- 905 47. Kamiran, F.; Calders, T. Data Preprocessing Techniques for Classification Without Discrimination.  
906 *Knowledge and Information Systems* **2012**, 33, 1–33. URL: <https://bit.ly/2lH95lQ>.
- 907 48. Zhang, B.H.; Lemoine, B.; Mitchell, M. Mitigating Unwanted Biases with Adversarial Learning.  
908 Proceedings of the 2018 AAAI/ACM Conference on AI, Ethics, and Society. ACM, 2018, pp. 335–340. URL:  
909 <https://arxiv.org/pdf/1801.07593.pdf>.
- 910 49. Zemel, R.; Wu, Y.; Swersky, K.; Pitassi, T.; Dwork, C. Learning Fair Representations. International  
911 Conference on Machine Learning, 2013, pp. 325–333. URL: <http://proceedings.mlr.press/v28/zemel13.pdf>.
- 913 50. Kamiran, F.; Karim, A.; Zhang, X. Decision Theory for Discrimination-aware Classification. 2012 IEEE 12th  
914 International Conference on Data Mining. IEEE, 2012, pp. 924–929. URL: <http://citeseerx.ist.psu.edu/viewdoc/download?doi=10.1.1.722.3030&rep=rep1&type=pdf>.
- 916 51. Rauber, J.; Brendel, W.; Bethge, M. Foolbox: A Python Toolbox to Benchmark the Robustness of Machine  
917 Learning Models. *arXiv preprint arXiv:1707.04131* **2017**. URL: <https://arxiv.org/pdf/1707.04131.pdf>.
- 918 52. Papernot, N.; Faghri, F.; Carlini, N.; Goodfellow, I.; Feinman, R.; Kurakin, A.; Xie, C.; Sharma, Y.; Brown,  
919 T.; Roy, A.; Matyasko, A.; Behzadan, V.; Hambardzumyan, K.; Zhang, Z.; Juang, Y.L.; Li, Z.; Sheatsley,  
920 R.; Garg, A.; Uesato, J.; Gierke, W.; Dong, Y.; Berthelot, D.; Hendricks, P.; Rauber, J.; Long, R. Technical  
921 Report on the CleverHans v2.1.0 Adversarial Examples Library. *arXiv preprint arXiv:1610.00768* **2018**. URL:  
922 <https://arxiv.org/pdf/1610.00768.pdf>.
- 923 53. Amershi, S.; Chickering, M.; Drucker, S.M.; Lee, B.; Simard, P.; Suh, J. Modeltracker: Redesigning  
924 Performance Analysis Tools for Machine Learning. Proceedings of the 33rd Annual ACM Conference on  
925 Human Factors in Computing Systems. ACM, 2015, pp. 337–346. URL: <https://www.microsoft.com/en-us/research/wp-content/uploads/2016/02/amershi.CHI2015.ModelTracker.pdf>.
- 927 54. Papernot, N. A Marauder’s Map of Security and Privacy in Machine Learning: An overview of current and  
928 future research directions for making machine learning secure and private. Proceedings of the 11th ACM  
929 Workshop on Artificial Intelligence and Security. ACM, 2018. URL: <https://arxiv.org/pdf/1811.01134.pdf>.
- 930 55. Mitchell, M.; Wu, S.; Zaldivar, A.; Barnes, P.; Vasserman, L.; Hutchinson, B.; Spitzer, E.; Raji, I.D.; Gebru,  
931 T. Model Cards for Model Reporting. Proceedings of the Conference on Fairness, Accountability, and  
932 Transparency. ACM, 2019, pp. 220–229. URL: <https://arxiv.org/pdf/1810.03993.pdf>.
- 933 56. Bracke, P.; Datta, A.; Jung, C.; Sen, S. Machine Learning Explainability in Finance: An Application  
934 to Default Risk Analysis **2019**. URL: <https://www.bankofengland.co.uk/-/media/boe/files/working-paper/2019/machine-learning-explainability-in-finance-an-application-to-default-risk-analysis.pdf>.
- 936 57. Friedler, S.A.; Scheidegger, C.; Venkatasubramanian, S.; Choudhary, S.; Hamilton, E.P.; Roth, D. A  
937 Comparative Study of Fairness-enhancing Interventions in Machine Learning. Proceedings of the  
938 Conference on Fairness, Accountability, and Transparency. ACM, 2019, pp. 329–338. URL: <https://arxiv.org/pdf/1802.04422.pdf>.
- 940 58. Schmidt, N.; Stephens, B. An Introduction to Artificial Intelligence and Solutions to the Problems of  
941 Algorithmic Discrimination. *Conference on Consumer Finance Law Quarterly Report* **2019**, 73, 130–144. URL:  
942 <https://arxiv.org/pdf/1911.05755.pdf>.
- 943 59. Hoare, C.A.R. The 1980 ACM Turing Award Lecture. *Communications* **1981**. URL: <http://www.cs.fsu.edu/~engelen/courses/COP4610/hoare.pdf>.